Technical Letter Report
TLR-RES/DE/REB-2021-16

Probabilistic Fracture Mechanics Application: FAVOR Case Study

Date:

September 2021

Prepared in response to Task 3 in User Need Request NRR-2016-004, by:

Nevin Martin
Michael J. Starr
Adah Zhang
Nathan W. Porter

Sandia National Laboratory

Patrick Raynaud

Senior Materials Engineer
Component Integrity Branch

Division of Engineering
Office of Nuclear Regulatory Research
U.S. Nuclear Regulatory Commission
Washington, DC 20555–0001

This report does not contain or imply legally binding requirements. Nor does this report establish or modify any regulatory guidance or positions of the U.S. Nuclear Regulatory Commission and is not binding on the Commission.

Probabilistic Fracture Mechanics Application: FAVOR Case Study

Manuscript Completed: January 2021
Date Published: September 2021

Prepared by:
Nevin Martin
Michael J. Starr
Adah Zhang
Nathan W. Porter

Sandia National Laboratories
P.O. Box 5800
Albuquerque, NM 87185

Patrick Raynaud, NRC Project Manager

U.S. Nuclear Regulatory Commission

Sandia National Laboratories is a multimission laboratory managed and operated by National Technology & Engineering Solutions of Sandia, LLC, a wholly owned subsidiary of Honeywell International Inc., for the U.S. Department of Energy's National Nuclear Security Administration under contract DE-NA0003525.

TABLE OF CONTENTS

INTRODUCTION

The origin of this PFM application study was a proposed presentation on a benchmarking study for SMiRT 25, “Use of Probabilistic Fracture Mechanics Calculations in Flaw Assessment – An Assessment of the Effect of Engineering Experience on Analytical Outcomes.” The study’s intent was to help formulate better guidance for regulatory and best-practices concerning the conduct and reporting of PFM analyses when applied to components of the primary pressure circuit of a nuclear reactor pressure vessel (RPV).

The hypothetical problem created for the benchmarking study involved two ultrasonic indications found close to the cladding in a nuclear RPV. The goal for participants was to quantify the risk of vessel failure when the vessel is subjected to a “normal” cooldown transient using Version 16.1 of the FAVOR computer code. This application study uses that hypothetical problem and follows the steps and actions presented in NUREG/CR-7278 [1].

1 STEP 1: TRANSLATION OF REGULATORY REQUIREMENTS INTO AN ANALYSIS PLAN

1.1 Step 1: Action 1 – Define the regulatory context

The goal of this analysis is to evaluate the acceptability of continued operations of a single Reactor Pressure Vessel (RPV) following a recent inspection which identified two indications (Figure 1-1) in the beltline region (hereafter referred to as Flaws A and B as defined in the figure). Both flaws were determined to be unallowable per ASME Section XI, IWB-3510, Allowable Planar Flaws (see Section 1.4 for additional details); as such, this analysis applies a probabilistic fracture mechanics PFM approach to determine the probability of failure of the RPV with the two indications subject to a normal cooldown transient. For this hypothetical example, the PFM approach is being proposed as an alternative under 10 CFR 50.55a(z) for continued plant operation.

1.2 Step 1: Action 2 – Define the QoI and how it relates to the model output and acceptance criteria

The Quantities of Interest (QoIs) are the Conditional Probability of Crack Initiation (CPI) and the Conditional Probability of Failure (CPF) at the current time (48 Effective Full Power Years (EFPY)), at the time of the next outage (50 EFPY), at the end of license (56.5 EFPY), and at a hypothetical license extension time (72 EFPY). These probabilities are estimated based on the RPV being subject to a normal cooldown transient as defined in Section 1.4.

The CPI and CPF are calculated internally in FAVOR and are output from the FAVPFM module of the code. A brief description of each is given below, with further details provided in [2]:

- CPI – The conditional probability of crack initiation is estimated by comparing the stress intensity factor, K_I, to the static cleavage fracture initiation toughness, K_{IC}, across the transient, where K_{IC} is defined as a distribution that is dependent on temperature and on RT_{NDT}. For a given transient, the temperature is time -dependent, and RT_{NDT} is a function of material chemistry and fluence, among other parameters.
- CPF – The conditional probability of failure is determined by estimating the probability that an initiated flaw will propagate through the RPV wall.

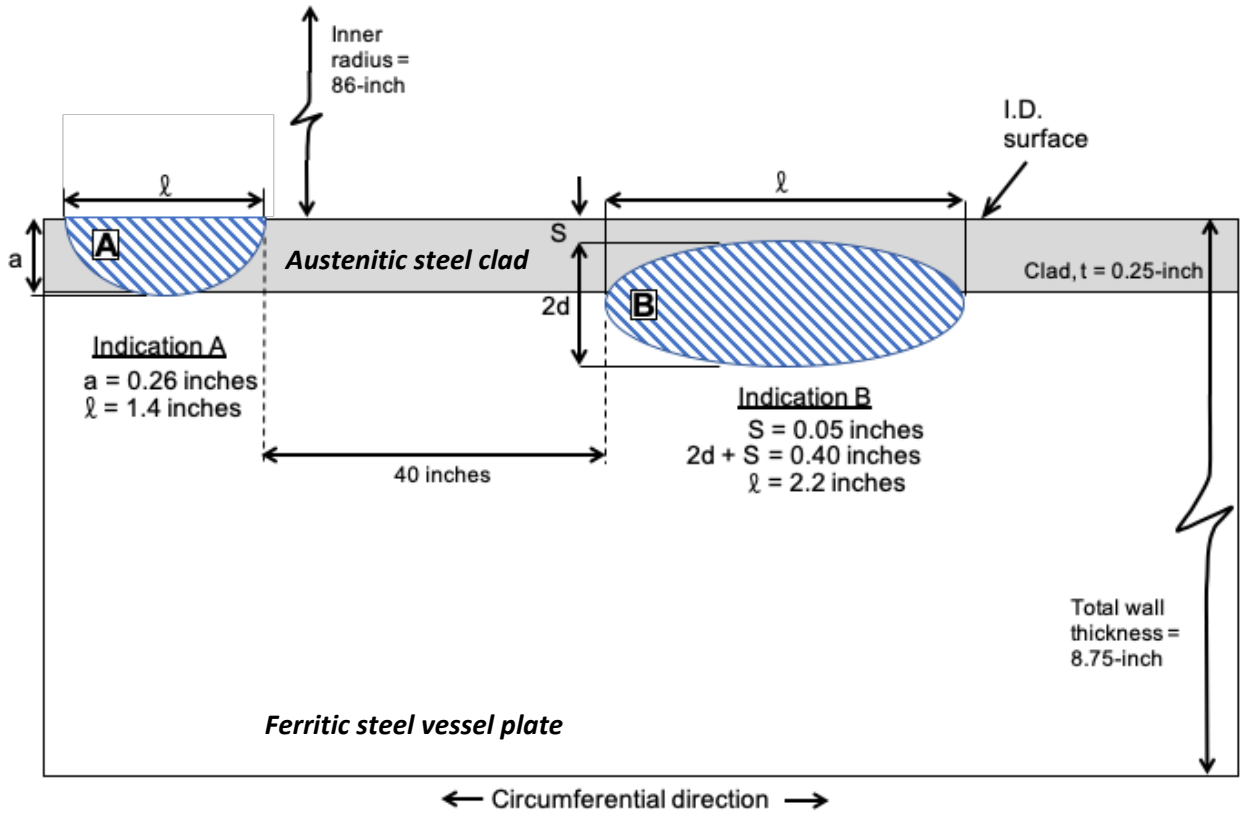

Figure 1-1: Schematic of flaw characterization.

Both probabilities are conditional based on the assumption that the cooldown transient occurs, and it is assumed that the probabilities calculated for Flaw A and Flaw B are statistically independent. The acceptance criterion for continued operations is not defined by the United States Nuclear Regulatory Commission (USNRC), although historically a frequency of 5×10^{-6} per year has been used for thru-wall crack frequency (TWCF) expressed in failed vessels per operating year. For the purposes of this analysis, the frequency of 1×10^{-6} failures per year acceptance criterion will be used, which is conservative over the frequency of 5×10^{-6} per year. Because the transient of interest in this study is a normal cooldown transient (see Section 1.4), the transient frequency is assumed to be 1 per year, and thus TWCF = CPF x event frequency (= 1/year) = CPF. As a result, in this report, CPF=TWCF is used as the metric to be compared against the failure criterion.

1.3 Step 1: Action 3 – Determine the suitability of PFM code for the specific application

The two flaws that were identified are in the beltline region of the RPV and it is of interest to assess the structural integrity of the RPV during normal operational transients (e.g., cooldown). Fracture Analysis of Vessels – Oak Ridge (FAVOR) version 16.1 was used for this analysis. FAVOR is an NRC-approved code that has been validated for this specific application under normal cooldown conditions. Details about the code can be found in [3] and [2].

1.4 Step 1: Action 4 – Identify key elements of the problem that impact analysis choices

There are several key elements that may impact analysis choices:

- Flaw characterization - The flaw category for both cracks can be determined through inspection of ASME Section XI, Figure IWB-3610-1: Characterization and Proximity Rules for Analytical Evaluation of Clad Components. Flaw A is a circumferential inner surface flaw. The total through-wall extent is 0.26 inches and the circumferential extent is 1.4 inches. Since the clad thickness is 0.25 inches, the flaw extends completely through the austenitic clad and into the ferritic steel vessel plate. Therefore, this flaw is deemed a Category 2 flaw (a surface flaw that penetrates through the cladding and into the ferritic steel).

  Flaw B is a circumferential embedded flaw. The total through-wall extent is 0.40 inches, with distance to ID surface of 0.05 inches and circumferential extent of 2.2 inches. Of course, this implies that the crack spans the clad and the vessel plate. Therefore, this is a Category 3 flaw (an embedded flaw very close to the surface, that straddles the cladding and the ferritic steel). A summary of Flaws A and B is given in Table 1-1.

Table 1-1: Flaw details

Flaw Indicator	Category	Type	a, Deepest Point of Crack[1] (in)	l, Flaw Width (in)	d or 2d, Extent of Through-Wall Cracking[2] (in)	S, Nearest ID Approach (in)	Aspect Ratio (AR)
A	2	Surface	0.26	1.4	0.26	0	5.385
B	3	Subsurface	0.40	2.2	0.35	0.05	5.5

[1] For surface cracks, a = d; for subsurface cracks, a = 2d + S.

[2] For surface cracks, d; for subsurface cracks, 2d

The determination of flaw size "allowability" is shown in Table 1-2. For Flaw Indicator A, the aspect ratio a/l can be calculated directly from Table 1-1. Linear interpolation was used to calculate the a/t ratio using the correct wall thickness column in ASME Table IWB-3510-1. The allowable flaw depth was then calculated directly using the vessel wall thickness of t = 8.75 inches. For Flaw A, the allowable flaw size is 0.2375 inches, smaller than the indicated depth. For Flaw B, the effective flaw characterization must first be determined. This is done by solving the inequality:

$$S \begin{cases} > 0.4d & \text{subsurface (a = d)} \\ \leq 0.4d & \text{surface (a = 2d + S)} \end{cases}$$

From the inequality, Flaw B is effectively a surface flaw with an allowable size of 0.2355 inches. Therefore, Flaw B is also deemed unallowable. In a real analysis, the assumption of a subsurface flaw for Flaw B would have to also be included as another alternative request under 10 CFR 50.55a(z) since under the surface proximity rules of the ASME Code, it is a surface flaw.

Table 1-2: Flaw allowability

Flaw Indicator	Effective Flaw Type	a/l	calculated using ASME Table IWB-3510-1		a, observed	Allowable
			a/t	**a, allowable**		
A	**Surface**	**0.186**	**0.02714**	**0.2375**	**0.26**	**No**
B	**Surface**	**0.182**	**0.02691**	**0.2355**	**0.40**	**No**

- Flaw geometry – The inspector identified the crack length and depth for both flaws in the inspection report, though there is some uncertainty on the precision of the tools used to estimate these geometries. Therefore, uncertainty in the flaw geometry is a key element to be considered in the analysis and it will be discussed in more detail in Section 2.1.
- Loading modeling – The transient that was assumed for this analysis was defined by the cooldown pressure and temperature measured at Plant 8 in 2007. A visual depiction of the cooldown transient is provided in Figure 1-2.

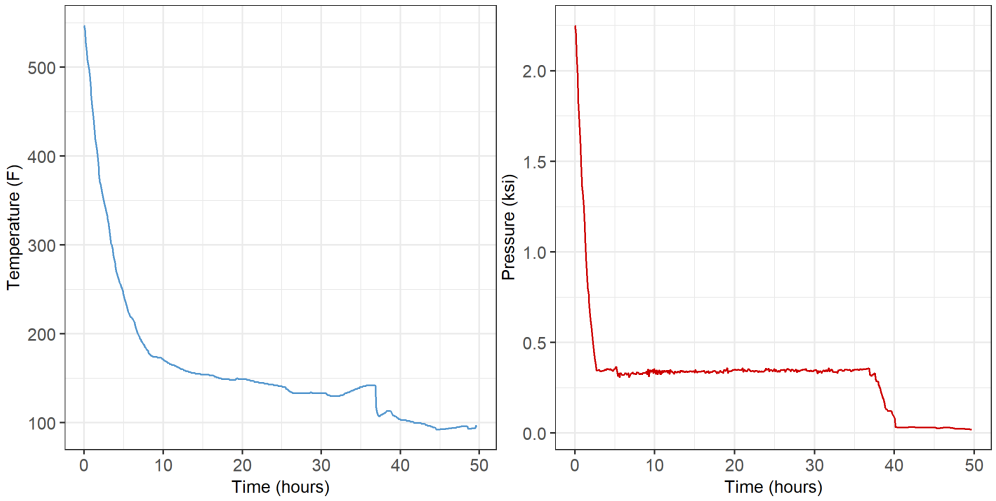

Figure 1-2: Cooldown temperature (left) and pressure (right) for Plant 8 as a function of time.

2 STEP 2: MODEL INPUT UNCERTAINTY CHARACTERIZATION

2.1 Step 2: Action 1 – Identify uncertain model inputs

2.1.1 Deterministic Inputs

Model inputs relating to the vessel geometry and thermo-elastic properties for the cladding and base materials are treated deterministically in this analysis. The RPV dimensions (i.e., internal radius (**IRAD**), thickness of wall (**W**) and cladding thickness (**CLTH**)) are considered well-defined per plant records. The thermo-elastic temperature-dependent inputs for the cladding and base materials are based on well-known material properties for the base (ferritic steel) and the cladding (austenitic stainless steel) according to the following sources [3]:

Base Steel

- Thermal conductivity – Table TCD – Material Group A – p. 592 [4]
- Thermal diffusivity – Table TCD – Material Group A – p. 592 [4]
- Young's Modulus of Elasticity – Table TM-1 – Material Group A – p. 606 [4]
- Coefficient of Expansion – Table TE-1 – Material Group D – p. 580-581 [4]
- Density = 489 lbm/ft^3 [4]

Cladding

- Thermal conductivity – Table TCD – High Alloy Steels – p. 598 [4]
- Thermal diffusivity – Table TCD – High Alloy Steels – p. 598 [4]
- Young's Modulus of Elasticity – NESC II Project – Final Report – p. 35 [5]
- Coefficient of Expansion – Table TE-1 – High Chrome Steels – p. 582-583 [4]
- Density = 489 lbm/ft^3 [4]

The base and cladding stress-free temperature (**T**) is defined as 488 °F based on [2]. Crack-face pressure loading (**CFP**) and both axial (**NRAX**) and circumferential (**NCRC**) residual stresses are turned on. The time period of the transient (**TOTAL)** is defined based on the cooldown transient described in Section 1.4 and the time increment (**DT**) was chosen as 1 minute based on a convergence study described in Section 3.2.

The distribution of flaws (**IPFLAW**) is specified as all surface-breaking flaws are internal, and category 3 flaws were not analyzed (**PC3_Option** set to 0) such that only embedded flaws in the first 1/8th of the wall thickness are considered (there were no other flaws in this analysis, so choosing these options allowed for quicker run times without otherwise changing the outcome of the analysis). Warm prestress (**WPS**) was turned off to impose a slight conservatism in our result based on uncertainty in the cooldown transient. While the WPS criteria might be satisfied by the transient used in the analysis, it was of interest to assess the results in the case the transient did not meet the criteria. The Eason 2006 [6] correlation was used for the correlation for irradiation shift calculations (**IRTNDT**) and ductile tearing (**IDT_OPTION**) was considered as a failure criterion for the ferritic steel (in addition to fracture mechanics driven failure). While a failure criterion (**FAILCR**) depth of 95% of the fraction wall thickness is recommended in [2], a value of 90% was used for this analysis, imposing a slight conservatism in what is considered a vessel failure.

Table 2-1 and Table 2-2 provide an exhaustive list of all deterministic inputs for the FAVLoad and FAVPFM input decks, respectively. Inputs with an asterisk were analyzed during a sensitivity study as described in Section 4.1. Additionally, the plate and weld embrittlement map was kept constant throughout the analysis and the full map is provided in APPENDIX B.

Table 2-1: Deterministic inputs - FAVLoad

Input	Description	Deterministic Value
IRAD	Internal Radius of RPV (in.)	86
W	Thickness of wall including cladding (in.)	8.75
CLTH	Cladding thickness (in.)	0.25
K	Base thermal conductivity (btu/hr-ft-°F)	24
C	Base specific heat (btu/lbm-°F)	0.120
RHO	Base density (lbm/ft^3)	489.00
E	Base elastic modulus (ksi)	28000
ALPHA	Base thermal expansion coefficient (1/°F)	0.00000777
NU	Base Poisson's ratio (-)	0.3
NTE	Base time-dependence flag off/on [0/1]	1
NK	Base thermal conductivity table	See APPENDIX B
NC	Base specific heat table	See APPENDIX B
NE	Base Young's modulus table	See APPENDIX B
NALF	Base coefficient of thermal expansion table	See APPENDIX B
K	Clad thermal conductivity (btu/hr-ft-°F)	10.0
C	Clad specific heat (btu/lbm-°F)	0.120
RHO	Clad density (lbm/ft^3)	489
E	Clad elastic modulus (ksi)	22800
ALPHA	Clad thermal expansion coefficient (1/°F)	0.00000945
NU	Clad Poisson's ratio	0.3
NT	Clad time-dependence flag off/on [0/1]	1
NK	Clad thermal conductivity table	See APPENDIX B
NC	Clad specific heat table	See APPENDIX B
NE	Clad Young's modulus table	See APPENDIX B
NALF	Clad coefficient of thermal expansion table	See APPENDIX B
T	Base and cladding stress-free temperature (°F)	488
CFP	Crack-face pressure loading applied off/on [0/1]	1
NRAX	Axial weld residual stresses off/on [0/101]	101
NCRC	Circ weld residual stresses off/on [0/101]	101
TOTAL	Time period for transient analysis (min)	2980
DT*	Time increment (min)	1
MTRAN	Number of transients to be input	1
ITRAN	PFM transient number	1
ISEQ	Thermal-hydraulic sequence number	1
NHTH	Time history table for the convective heat transfer coefficient (btu/hr-ft^2-°F)	Constant: 10,000
NTTH*	Time history definition for the coolant temperature	See Figure 1-2
NPTH	Time history definition for the coolant pressure	See Figure 1-2

Table 2-2: Deterministic inputs - FAVPFM

Input	Description	Deterministic Value
NSIM*	Number of RPV simulations	20000
IPFLAW	Distribution of surface-breaking and embedded flaws	SB internal, embedded uniform in inner 3/8th
IGATR	Applied per flaw in the *Initiation-Growth-Arrest* (IGA) model	100
WPS_OPTION*	Warm prestress (off/on) [0/1]	0
PC3_OPTION	Sets calculations for category 3 flaws	0
CHILD_OPTION	Sets child subregions	1
IRTNDT*	Correlation for irradiation shift calculations	2006
TC	Normal operating coolant temperature	532
EFPY	Effective full power years	48, 50, 56.5, or 72
IDT_OPTION	Ductile tearing in IGA submodel (off/on) [0/1]	1
IDT_INI	Additional reporting for flaw initiation due to ductile tearing (off/on) [0/1]	0
ILONG_OUT	Additional reporting for contribution to CPI and CPF from the major regions in the belt line (off/on) [0/1]	0
FLWSTR*	Flow stress (ksi)	80
USKIA*	Upper bound KIc and Kia (ksi/in^1/2)	200
KIa_MODEL	Arrest model for checking stable arrest	Model based on CCA + large specimen data
LAYER_OPT	Weld layer resampling option	0
FAILCR*	Vessel failure criterion (fraction of total wall thickness)	0.9

2.1.2 Uncertain Inputs

There are two sources of uncertainty that are considered in the probabilistic analysis – uncertainty due to flaw location and geometry, and uncertainty due to fluence and embrittlement.

Flaw location and geometry. Due to limitations in the accuracy and resolution of the inspection tools used to characterize the flaws, uncertainty was introduced into the flaw depths and lengths of Flaws A and B. As a result of the uncertainty in flaw dimensions, uncertainties regarding whether the flaws should be considered surface breaking or embedded, as well as regarding the aspect ratios of the flaws, were considered. These uncertainties were ultimately reflected in the generation of the flaw file distributions that are taken as input into the FAVPFM module of FAVOR. FAVOR then internally samples from the flaw file distributions and propagates the samples through the model. Details on this process is provided in Section 2.2.

Fluence and embrittlement. Fluence and embrittlement related parameters – nickel, manganese, copper, phosphorous, neutron fluence and uncertainties in the unirradiated $RT_{NDT(0)}$ are sampled from distributions that are intrinsic to the FAVOR code [2]. Additionally, the classification of aleatory and epistemic uncertainties in the unirradiated $RT_{NDT(0)}$ is also made internally in FAVOR. The choice of these distributions and the characterization of uncertainties was assumed to be sufficient per NRC's approval of the FAVOR code.

FAVOR takes as input into the FAVPFM module the standard deviations of the normal sampling distributions for the weld and plate chemistries. These standard deviations were chosen based on recommended values in the FAVOR User's Guide [3] and are shown in Table 2-3. Again, an asterisk by the parameter name indicates that a sensitivity study was performed on this parameter in Section 4.

Table 2-3: Fluence and embrittlement parameters

Parameter	Description	Value
SIGFGL*	Fluence standard deviation	0.118
SIGFLC*	Local fluence standard deviation	0.056
WSIGCU	Copper standard deviation in weld	0.167
WSIGNI	Nickel standard deviation in weld	0.162
WSIGP	Phosphorous standard deviation in weld	0.0013
PSIGCU	Copper standard deviation in plate	0.0073
PSIGNI	Nickel standard deviation in plate	0.0244
PSIGP	Phosphorous standard deviation in plate	0.0013

2.2 Step 2: Action 2 – Specify probability distributions on uncertain inputs

It was decided that flaw dimensions would be considered uncertain inputs. Consequently, a scheme for creating different flaw files was sought, ideally through linking any distributions or bounds on parameters to realistic observations or flaw detection capabilities. From the SMiRT problem description we have the following:

Flaw A: depth = 0.26 inches, length = 1.4 inches, AR = 5.38, norm_depth = 0.0297

Flaw B: depth = 0.40 inches, length = 2.2 inches, AR = 5.5, norm_depth = 0.0457

For deterministic analysis, this led to considering the flaws as inner surface breaking with aspect ratio, AR = 6. This is one of the discrete allowable aspect ratios for FAVOR analyses and the practice of rounding upward yields conservative predictions. The normalized flaw depths (flaw depth divided by vessel thickness) chosen for analysis were Flaw A = 0.03 and Flaw B = 0.05. Of note for this analysis, Flaw B was defined as an embedded flaw in the problem statement but is treated as a surface-breaking flaw using ASME SC-XI flaw sizing guidance, IWB-3600 (alternatively, Flaw B could be treated like an embedded flaw using the appropriate flaw file structure as defined in a FAVOR analysis).

In the course of arriving at rational bounds or distributions on the flaw length and depth, some potential considerations are:

- accuracy and resolution of inspection tools
- crack categorization (e.g. surface breaking or embedded)
- scheme for assigning flaws to AR and normalized depth bins
- crack front proximity to clad

Several generalized sampling schemes were considered and included as possible parameterizations in the source derivations. For the purposes of demonstration for this application study, the uncertainty of the actual dimensions of each of the flaws was parameterized with a generalized uncertainty, ε, where $0 \leq \varepsilon \leq 1$. The bounds for each of the five flaw parameters: (1) Flaw A crack front depth, (2) Flaw A crack length, (3) Flaw B outer crack front depth, (4) Flaw B inner crack front depth, and (5) Flaw B length are given below.

$$a_{depth} = [\max[0.25 \quad 0.26(1-\varepsilon)] \quad 0.26(1+\varepsilon)]$$

$$a_{length} = [1.40(1-\varepsilon) \quad 1.40(1+\varepsilon)]$$

$$b_{outer\_depth} = [\max[0.25 \quad 0.40(1-\varepsilon)] \quad 0.40(1+\varepsilon)]$$

$$b_{inner\_depth} = [\max[0 \quad 0.05-0.2\varepsilon] \quad \min[0.05+0.2\varepsilon \quad 0.249]]$$

$$b_{length} = [2.20(1-\varepsilon) \quad 2.20(1+\varepsilon)]$$

For example, if the generalized uncertainty for Flaw A depth is $\varepsilon = 0.5$, then the lower bound for the crack depth is the maximum of [0.25 0.13] and the upper bound for the crack depth is 0.39. So, the bounds are

$$0.25 \leq a_{depth} \leq 0.39$$

Once the bounds for each of the uncertain parameters have been established, then a probability distribution on those bounds can be defined. For all FAVOR simulations, it was assumed that the same generalized uncertainty was applied to each variable and the same distribution was applied to each variable. In general, though, this is not required and unique ε and distributions could be used for each variable. Two distributions were considered: uniform on the bounded interval and normal on the interval with the 3rd standard deviation aligned with the interval bounds.

3 STEP 3: ESTIMATION OF QOI AND ASSOCIATED UNCERTAINTY

3.1 Step 3: Action 1 – Select a sampling scheme

The generation of the flaw files is computationally efficient, so one million simple random samples from the flaw depth and length distributions are used to construct them. To guarantee that the statistics always produce the expected number of existing flaws, the flaw density is scaled to produce 0.1% more than the expected number (FAVOR internally rounds down to the closest whole number).

For each sample of crack depth and crack length, a corresponding aspect ratio was estimated using the following binning scheme for surface-breaking flaws:

- AR < 2 get binned in AR = 2
- 2 ≤ AR ≤ 6 get binned in AR = 6

- 6 ≤ AR ≤ 10 get binned in AR = 10
- AR > 10 get binned in AR = ∞

The four discrete aspect ratio bins are hard-coded into the FAVOR flaw file input structure for surface-breaking flaws. For embedded flaws, the FAVOR-defined aspect ratio bin structure is different than that used for surface-breaking flaws; there are ten aspect ratio intervals for embedded flaws. In all cases the crack depth was rounded to the nearest discrete crack depth defined in the FAVOR input structure.

This resulted in a distribution of crack depths and aspect ratios that were used to generate the flaw file that is inputted into FAVPFM. A MATLAB post processing script was used for the sampling and generation of the flaw files; this script is available to the NRC upon request.

3.2 Step 3: Action 2 – Assess sampling uncertainty: statistical convergence analysis

Two parameters were assessed for convergence purposes: the time increment (**DT**) used in the time integration in FAVPFM and the number of simulations (**NSIM**). This section describes the convergence studies that were performed for each of these parameters.

Time integration time increment (DT). Many cases were run to assess the convergence of CPI and CPF with respect to DT. These cases were run for 48 EFPY using the default parameters in Table 2-1, Table 2-2, and Table 2-3 and the nominal crack depths and aspect ratios for flaws as defined in Table 1-1. The uncertain inputs are defined by a normal distribution as defined in Section 2.2 with the uncertainty parameter $\varepsilon = 0.25$. This study was conducted for two cases: the 2007 Plant 8 normal cooldown transient and the ASME maximum cooldown pressure-temperature as defined by Appendix G of ASME SC-XI. Analyzing the convergence of the ASME maximum cooldown transient allows the assessment of a case which produces higher values of CPI and CPF, indicating that the convergence behavior may extend beyond the case considered in this document. The results are summarized in Figure 3-1, indicating that the mean CPI and CPF converge as the time step is decreased. Therefore, a time increment of 1.0 is selected, which balances simulation expense with the convergence of CPI and CPF.

Number of simulations (NSIM). Convergence of the CPI and CPF based on the number of simulations was assessed using the inputs defined in Table 2-1, Table 2-2, and Table 2-3 and accounting for uncertainty in the crack depths and lengths ($\varepsilon = 0.25$). The converged value of DT=1 was used for this analysis. This convergence analysis was performed at 48 EFPY using the normal cooldown transient. Two methods were used to assess convergence.

First, the mean and 99th percentile CPI and CPF were plotted as function of the number of simulations. The mean is output directly from FAVPFM and the 99th percentile is estimated from an exponential distribution fit to the samples. The results are provided in Figure 3-2. Both estimates are mostly converged after 20,000 simulations, which is the sample size selected for the final analysis.

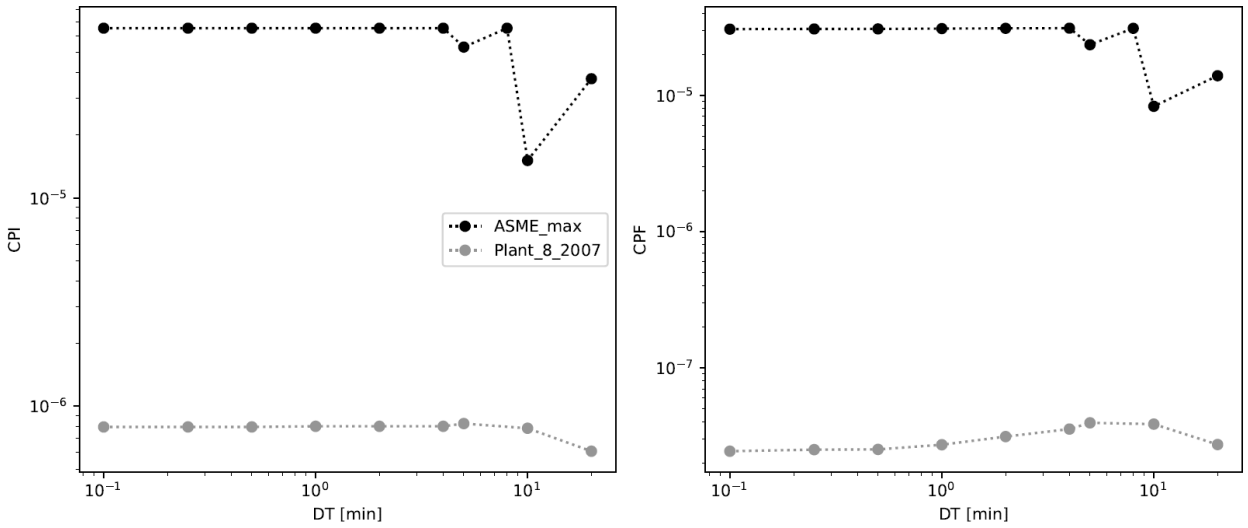

Figure 3-1: Convergence analysis of CPI and CPF as DT is refined for the 2007 Plant 8 and ASME maximum cooldown transients.

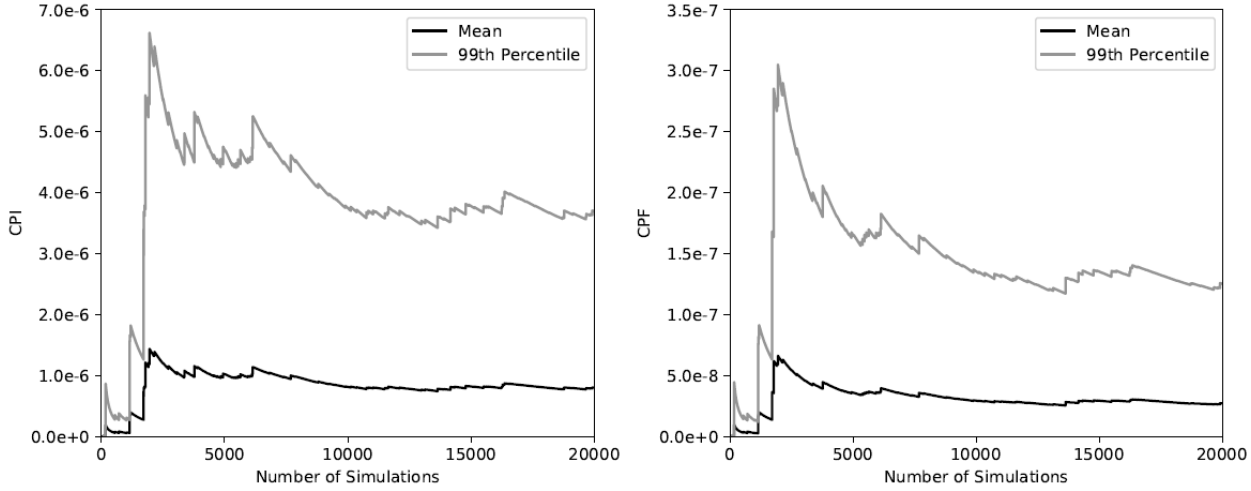

Figure 3-2: Mean and 99th percentile of CPI (left) and CPF (right) versus the number of simulations.

The second approach was to generate a statistical confidence bound around the mean and 99th percentile of the CPI and CPF to provide a quantitative measure of the statistical uncertainty in the estimates. This confidence bound was produced using a bootstrap procedure [7] that used the sampled CPI and CPF to estimate sampling uncertainty using 20,000 simulations. Here, the statistical results are resampled with replacement 1,000 times. For each resample, the mean and 99th percentile are estimated from 10,000 samples. Statistical uncertainty in the estimators can be approximated using summary statistics of the 1,000 bootstrap samples. A histogram of the mean and 99th percentile estimates are provided in Figure 3-3 and Figure 3-4, respectively. For each plot of the CPI or CPI, 95% confidence intervals are provided from the bootstrap analysis. These bounds have the interpretation that upon repeated samples, the mean CPI would fall in the interval [5.46e-7, 1.09e-6] and the mean CPF would fall in the interval [1.71e-8, 3.83e-8] 95% of the time. Similarly, 95% percent of the time, the 99th percentile of CPI and CPF would fall in the interval [2.51e-6, 5.03e-06] and [7.86e-8, 1.76e-07], respectively.

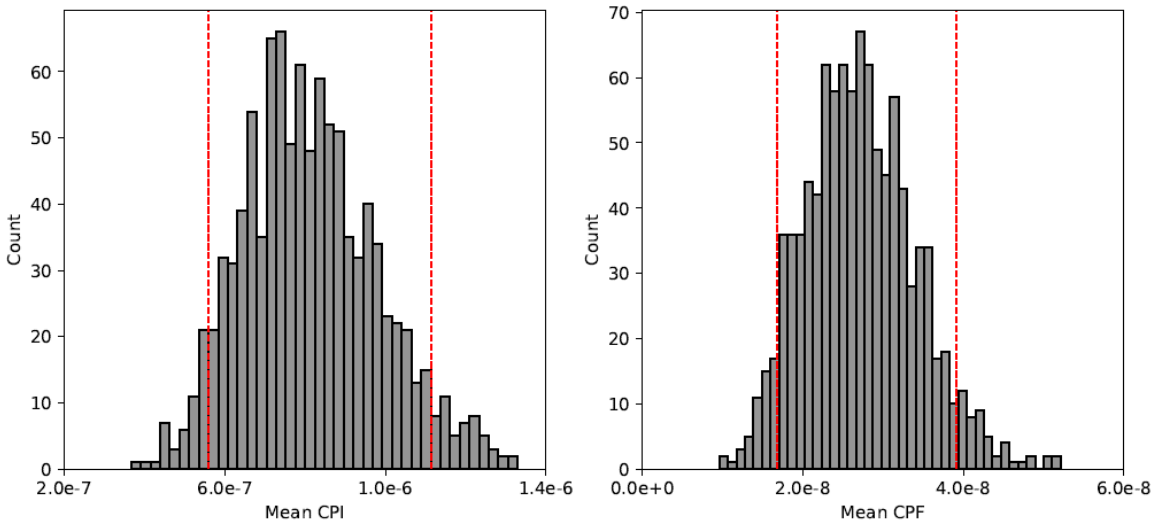

Figure 3-3: 95% sampling uncertainty confidence intervals for the mean CPI (left) and CPF (right).

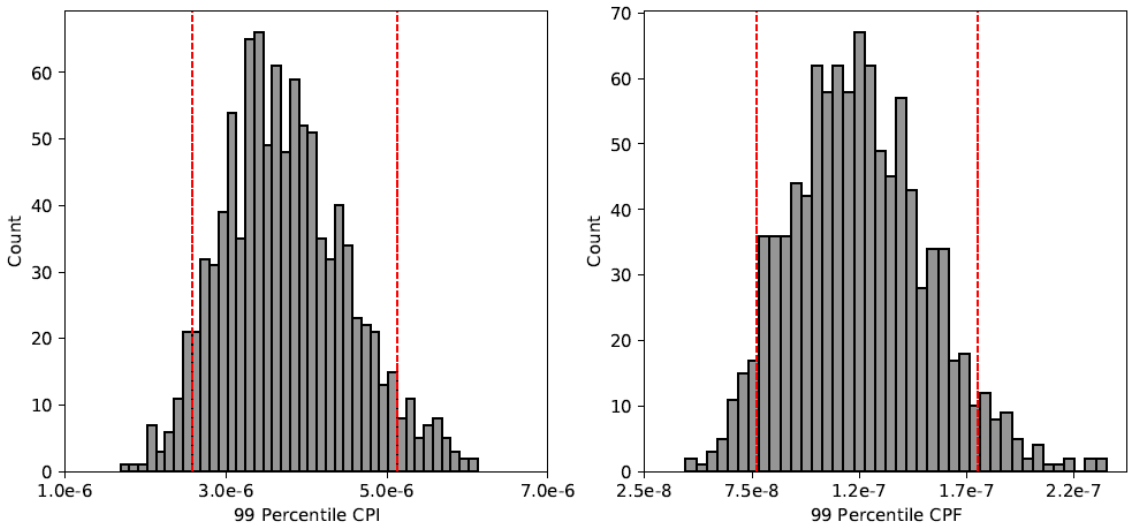

Figure 3-4: 95% sampling uncertainty confidence intervals for the 99th percentile CPI (left) and CPF (right).

3.3 Step 3: Action 3 – Conduct sensitivity analyses: input uncertainty importance determination

As FAVOR does not provide the sampled values of the uncertain inputs that are sampled internally in the code, a traditional sensitivity analysis was not conducted. However, several sensitivity studies were performed to assess the effect of different modeling assumptions on the CPI and CPF. Details are provided in Section 4.

3.4 Step 3: Action 4 – Output uncertainty analysis

FAVOR was run using the inputs defined in Section 2 for the Plant 8 2007 normal cooldown transient at 48, 50, 56.5, and 72 EFPY. Uncertainty was considered in the crack depth and length for both flaws, as well as in the fluence and embrittlement parameters. The uncertainties are characterized by the normal distribution defined in Section 2.2 with the uncertainty parameter $\varepsilon = 0.25$. A summary of the results is presented in Table 3-1. Here, the mean and 99th percentile of CPI and CPF are shown for all four EFPYs. Additionally, a 95% confidence interval upper bound on the 99th percentile gives an upper bound on the percentile after accounting for sampling uncertainty.

As established in Section 1.2, the acceptance criterion for CPF is 1e-6. For all EFPY cases, the mean CPF and 99th percentile of CPF are about two and one magnitude smaller than the criterion, respectively. Therefore, this analysis indicates that all cases are acceptable, even in the presence of uncertainty. Additionally, because the 95% upper bound on the 99th percentile is smaller than the acceptance criterion, the statistical uncertainty in the 20,000 samples is not sufficiently large to cause unacceptable results for any case.

Table 3-1: Output uncertainty analysis results

	CPI			CPF		
EFPY	Mean	99th Percentile	95% Upper Bound on 99th Percentile	Mean	99th Percentile	95% Upper Bound on 99th Percentile
48	8.01e-7	3.74e-6	5.13e-6	2.72e-8	1.25e-7	1.80e-7
50	8.38e-7	3.87e-6	5.39e-6	2.83e-8	1.31e-7	1.88e-7
56	9.57e-7	4.39e-6	6.01e-6	3.56e-8	1.63e-7	2.23e-7
72	1.15e-6	5.33e-6	7.20e-6	4.94e-8	2.28e-7	3.17e-7

4 STEP 4: SENSITIVITY STUDIES TO ASSESS CREDIBILITY OF MODELING ASSUMPTIONS

4.1 Step 4: Action 1 – Determine set of sensitivity studies

Several sensitivity studies were performed to assess the effect on the CPI and CPF when changing analysis assumptions. Prior to conducting the studies, an initial "default" run was performed using the ASME maximum cooldown pressure-temperature at 48 EFPY with the input values shown in Figure 4-1. This default case was used to compare the results of plausible alternate assumptions for several of the inputs. The flaw depths and aspect ratios were fixed at a single value as defined in Table 1-1. The mean CPI and CPF for the default case were estimated at 5.376e-05 and 2.449e-05, respectively.

Table 4-1 provides an overview of the parameters that were considered for the sensitivity studies, along with their default values and possible ranges.

```
*****************************************************************************************************
CNT1 NSIM=10000 IPFLAW=1  IGATR=100    WPS_OPTION=1    PC3_OPTION=0    CHILD_OPTION=1   RESTART_OPTION=0
CNT2 IRTNDT=2006 TC=532 EFPY=48  IDT_OPTION=1  IDT_INI=0  ILONG_OUT=0
CNT3 FLWSTR=80.  USKIA=200. KIa_Model=2  LAYER_OPTION=0  FAILCR=0.9
GENR SIGFGL=0.118 SIGFLC=0.056
SIGW WSIGCU=0.167   WSIGNI=0.162    WSIGP=0.0013
SIGP PSIGCU=0.0073   PSIGNI=0.0244   PSIGP=0.0013
TRAC ITRAN=1  IRPV=1  KFLAW=1   FLAW_LOG_OPTION=0
LDQA IQA=0 IOPT=1 IFLOR=2 IWELD=1 IKIND=1 XIN=0.05 XVAR=0.40 ASPECT=999
DTRF NT=0
WELD NWSUB=7     NWMAJ=7
PLAT NPSUB=6     NPMAJ=6
*=============================================================================================*
* 1   2   3    4       5     6     7      8     9    10 11  12  13    14    15    16   17   18  19  20
*****************************************************************************************************
*sub left right mj neutron                                    RTu  RTu    PF  angle  ht  fusion weld
* no  sub  sub reg fluence  cu     ni    phos   mang  flags    (1sig)      (deg) (in)  area  ornt NA Charpy
*****************************************************************************************************
  1     8   9   1   2.1241 0.213  1.01  0.019   1.315 1  3  -56.  17    1  0.96  60.7  516   1  0  111
  2     9  10   2   2.6524 0.213  1.01  0.019   1.315 1  3  -56.  17    1  0.96  60.7  516   1  0  111
  3    10   8   3   2.6524 0.213  1.01  0.019   1.315 1  3  -56.  17    1  0.96  60.7  516   1  0  111
  4    11  12   4   2.6802 0.213  1.01  0.019   1.315 1  3  -56.  17    1  1.16  94.0  799   1  0  111
  5    12  13   5   2.1408 0.213  1.01  0.019   1.315 1  3  -56.  17    1  1.16  94.0  799   1  0  111
  6    13  11   6   2.6802 0.213  1.01  0.019   1.315 1  3  -56.  17    1  1.16  94.0  799   1  0  111
*****************************************************************************************************
  7     8  11   7   3.4041 0.203 1.018  0.013   1.147 2  2  -56   17    1  360  1.3125 4833   2  0  111
*****************************************************************************************************
  8     8   8   8   3.4010 0.190  0.48  0.016   1.24  0  0    0    0    2 119.04 60.7   0    0  0  115
  9     9   9   9   3.4010 0.190  0.50  0.015   1.24  0  0  -30    0    2 119.04 60.7   0    0  0  115
 10    10  10  10   3.4010 0.120  0.55  0.010   1.27  0  0  -25    0    2 119.04 60.7   0    0  0  115
 11    11  11  11   3.4346 0.240  0.51  0.009   1.24  0  0   -5    0    2 118.84 94.0   0    0  0  115
 12    12  12  12   3.4346 0.240  0.50  0.010   1.35  0  0  -30    0    2 118.84 94.0   0    0  0  115
 13    13  13  13   3.4346 0.240  0.50  0.011   1.29  0  0   -5    0    2 118.84 94.0   0    0  0  115
*=============================================================================================*
*****************************************************************************************************
```

Figure 4-1: Default inputs for sensitivity studies.

Table 4-1: Parameters for sensitivity studies

Parameter	Description	Default	Range
IGATR	Initiation Growth Arrest model flag	100	[100 1000]
WPS_OPTION	Warm pre-stress model flag	1 (warm prestress mode 1)	[0,1,2,3]
IRTNDT	NDT model	2006	[992,2000,2006,20071, 20072,20073]
IDT_OPTION	Ductile tearing flag	1 (use ductile tearing)	[0,1]
FLWSTR	Flow stress	80	[60 100] (arbitrary)
KIa_Model	KIa curve	2	[1,2]
FAILCR	Through wall depth failure	0.9	[0.25 0.95]
SIGFGL	SD multiplier best estimate fluence	0.118	0.118±25%
SIGFLC	SD multiplier mean fluence	0.056	
Flaw File	file that defines flaw sampling details	Two flaws, uniform distribution at 0.03t and 0.05t, all of AR = 6	Various definitions

4.2 Step 4: Action 2 – Conduct studies and present results

Table 4-2 provides an exhaustive list of all the sensitivity studies that were performed along with the estimated mean CPI and CPF for each study. These inputs were studied as there was not a strong basis for choosing their values and it was of interest to understand how these inputs might affect the conclusions of the analysis. For each entry in the table, only one input was perturbed from the default case. All inputs were analyzed for the 48 EFYP transient for the normal cooldown with uncertain parameters set to a normal distribution defined by $\varepsilon = 0.25$. Inputs that did not have a significant effect on the response include the flow stress (**FLWSTR**) and the fluence standard deviations (**SIGFGL** and **SIGFLC**). The remaining inputs had an impact on the mean CPI and/or CPF and were set based on FAVOR input recommendations or to achieve conservatism in the resulting probability estimates.

The number of initiation-growth-arrest trials per flaw (**IGATR**) had an impact on both CPI and CPI, but it was fixed at 100 based on FAVOR input recommendations. Warm prestress (**WPS**) had an effect on both the mean CPI and CPF; however, as mentioned above, it was decided to turn off warm prestress in the final analysis to impose some conservatism due to uncertainty that may be present in the cooldown transient. The choice of correlation used for the irradiation shift calculations (**IRTNDT**) had some effect on mean CPI and CPF, though the Eason 2006 method was chosen for the final analysis because this correlation is believed to be the most accurate at high fluence, given current data. In addition, the Eason 2000 method is results in the highest CPI and CPF, and therefore it is conservative. The ductile tearing off (**IDT_OPTION**) did affect the simulation, so it is set at the more conservative value. Unsurprisingly, the failure criterion (**FAILCR**) has a large effect on the mean CPF. As mentioned in Section 2.1.1, this was fixed at 0.9 based on a slight conservatism over FAVOR recommendations.

Table 4-2: Mean CPI and CPF for all sensitivity studies

Case	Parameter	Mean CPI	Mean CPF	Notes
DEFAULT		8.015e-7	2.721e-8	
1	IGATR = 1000	1.020e-6	3.065e-8	
2	WPS_OPTION = 0	8.583e-7	2.830e-8	
	WPS_OPTION = 2	8.367e-7	2.678e-8	
	WPS_OPTION = 3	3.435e-7	1.260e-8	
3	IRTNDT = 992	6.362e-7	1.258e-8	Regulatory Guide 1.99 Rev. 2 correlation
	IRTNDT = 2000	5.966e-7	1.502e-8	Eason 2000 correlation
	IRTNDT = 20071	4.720e-7	1.031e-8	Kirk 2007 correlation
	IRTNDT = 20072	1.394e-7	6.221e-10	RADAMO 2007 correlation
	IRTNDT = 20073	3.744e-7	8.209e-9	EasonKirk/RADAMO 2007 correlation
4	IDT_OPTION = 0 (KIa_Model = 2)	8.015e-7	2.721e-8	KIa model based on CCA + large specimen data
5	FLWSTR = 60	8.015e-7	2.721e-8	
	FLWSTR = 100	8.015e-7	2.721e-8	

Case	Parameter	Mean CPI	Mean CPF	Notes
6	IDT_OPTION = 0 (KIa_Model = 1)	8.015e-7	3.005e-14	KIa model based on CCA specimens
7	FAILCR = 0.25	8.015e-7	7.551e-7	
	FAILCR = 0.50	8.015e-7	5.275e-8	
	FAILCR = 0.75	8.015e-7	2.849e-8	
8	SIGFGL = 0.1475 (+25%)	8.003e-7	2.755e-8	Fluence standard deviation increased by 25% of nominal value
	SIGFGL = 0.0885 (-25%)	8.021e-7	2.767e-8	Fluence standard deviation decreased by 25% of nominal value
9	SIGFLC = 0.07 (+25%)	8.016e-7	2.725e-8	Local fluence standard deviation increased by 25% of nominal value
	SIGFLC = 0.042 (-25%)	8.014e-7	2.699e-8	Local fluence standard deviation decreased by 25% of nominal value
10	Flaw A = 2 x Flaw B	2.134e-6	6.362e-8	Double the distribution of Flaw A compared to Flaw B
	2 x Flaw A = Flaw B	6.195e-7	2.057e-8	Double the distribution of Flaw B compared to Flaw A
	AR = 2	0	0	All flaws have aspect ratio 2
	AR = 6	4.314e-7	1.365e-8	All flaws have aspect ratio 6
	AR = 10	2.106e-6	6.457e-8	All flaws have aspect ratio 10
	AR = ∞	1.742e-5	5.792e-7	All flaws have infinite aspect ratio
	0.02t	0	0	All flaws at 0.02t
	0.03t	2.933e-6	8.385e-8	All flaws at 0.03t
	0.04t	5.133e-7	1.940e-8	All flaws at 0.04t
	0.05t	0	0	All flaws at 0.05t
	0.25t	0	0	All flaws at 0.25t

The choice of flaw depth, distribution, and aspect ratio (as described in Case 10) had a large effect on the mean CPI and CPF. This result prompted the incorporation of additional uncertainty for the flaw depths and lengths, described in Section 2.1.2, as uncertainty due to limitations in the inspector's tools may result in increased uncertainty in the CPI and CPF estimates. Two additional sensitivity studies were performed to assess the effect of different assumptions that were required in the generation of the flaw files after incorporating crack depth and length uncertainty:

1) The distributional form of the uncertainty was set to either uniform or normal on a bounded interval, and
2) The categorization of the flaws as either surface-breaking or embedded.

4.2.1 Flaw sample distributions

Using the sampling scheme previously introduced in Section 2.2, a total of four unique scenarios were considered:

1. Flaw parameters uniformly sampled with both flaws assumed surface-breaking
2. Flaw parameters sampled from a normal distribution with both flaws assumed surface-breaking
3. Flaw parameters uniformly sampled with Flaw B either surface-breaking or embedded as calculated from sampled dimensions and Flaw A surface breaking
4. Flaw parameters sampled from a normal distribution with Flaw B either surface-breaking or embedded as calculated from sampled dimensions and Flaw A surface breaking

Scripts were used to generate the flaw files, which guarantees that the required minimum densities were achieved and two flaws were produced for each simulation. The sampled scheme was also coded to preclude the sampling of non-physical crack parameters. New flaw files were created, and the FAVOR analyses were re-run. The results for mean CPI and mean CPF are given in Table 4-3 and Table 4-4, respectively. In general, the probability of crack initiation and of failure increase slightly as the parameter uncertainty increases. Note that for the sampling scheme used, the uncertainty in the flaw parameters has been parameterized through the normalized parameter, ε, defined previously in Section 2.2. With this flaw file creation methodology, embedded flaws don't exist (i.e., have zero probability) until reaching uncertainties of 0.05 and 0.10 under normal and uniform sampling, respectively.

Table 4-3: Mean CPI for distributed flaw files with various parameter uncertainty

Parameter Uncertainty ε	Surface-Breaking		Mixed	
	Uniform (Scenario 1)	Normal (Scenario 2)	Uniform (Scenario 3)	Normal (Scenario 4)
0.00	9.369e-7	9.369e-7	9.369e-7	9.369e-7
0.01	9.369e-7	9.369e-7	9.369e-7	9.369e-7
0.05	9.369e-7	9.369e-7	9.369e-7	9.369e-7
0.10	1.224e-6	9.959e-7	4.863e-7	3.682e-7
0.20	1.511e-6	1.482e-6	5.890e-7	4.379e-7
0.25	1.487e-6	8.015e-7	6.162e-7	8.149e-7
0.50	2.116e-6	2.174e-6	7.426e-7	8.890e-7
1.00	2.572e-6	1.744e-6	3.416e-6	7.708e-6

Table 4-4: Mean CPF for distributed flaw files with various parameter uncertainty

Parameter Uncertainty ε	Surface-Breaking		Mixed	
	Uniform (Scenario 1)	Normal (Scenario 2)	Uniform (Scenario 3)	Normal (Scenario 4)
0.00	3.004e-8	3.004e-8	3.004e-8	3.004e-8
0.01	3.004e-8	3.004e-8	3.004e-8	3.004e-8
0.05	3.004e-8	3.004e-8	3.004e-8	3.004e-8
0.10	3.880e-8	3.202e-8	1.630e-8	1.170e-8
0.20	4.849e-8	4.478e-8	1.927e-8	1.432e-8
0.25	4.659e-8	2.721e-8	1.995e-8	2.651e-8
0.50	6.347e-8	6.591e-8	2.140e-8	2.818e-8
1.00	9.834e-8	5.289e-8	1.164e-7	3.297e-7

An intrinsic feature of using parameter uncertainty to capture the uncertainty of the physical dimensions of the indicated flaws is the relationship between flaw size and failure probability. A series of visualizations of the relationship between flaw characteristics and parameter uncertainty are shown in the APPENDIX A. Figure 4-2 and Figure 4-3 use those data along with selected results provided in Table 4-3 and Table 4-4 to plot the empirical CDFs of flaw distributions for families of parameter uncertainty, ε, for mean CPI and mean CPF, respectively. The figures show the results obtained with surface-breaking flaws sampled from normal distributions (Scenario 2). The plots are a quantitative demonstration of the relationship between parameter uncertainty, flaw depth distribution, and the resultant probabilities of either crack initiation or vessel failure. A general qualitative observation is that increasing parameter uncertainty yields increased flaw density at larger flaw depths, which correlates with larger predictions of mean CPI and CPF. Note that although the flaw characteristics were sampled continuously, FAVOR employs a binned input structure. Consequently, the plotted flaw depth CDFs are discontinuous.

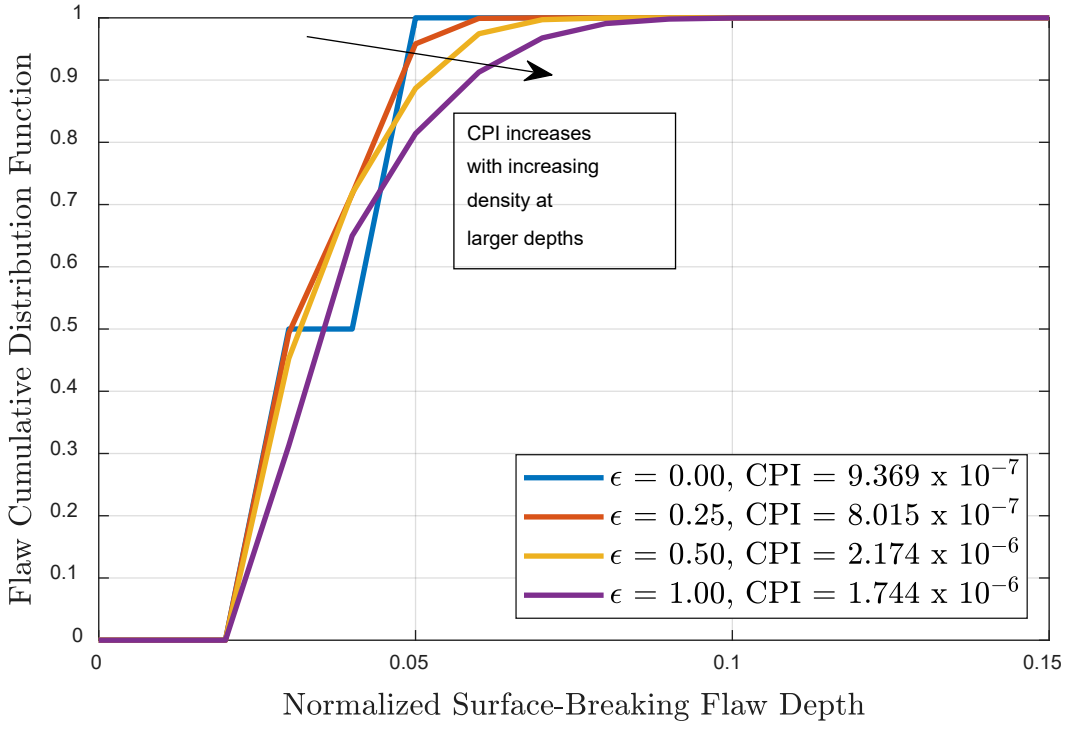

Figure 4-2: Empirical CDFs of flaw distributions for families of parameter uncertainty for mean CPI.

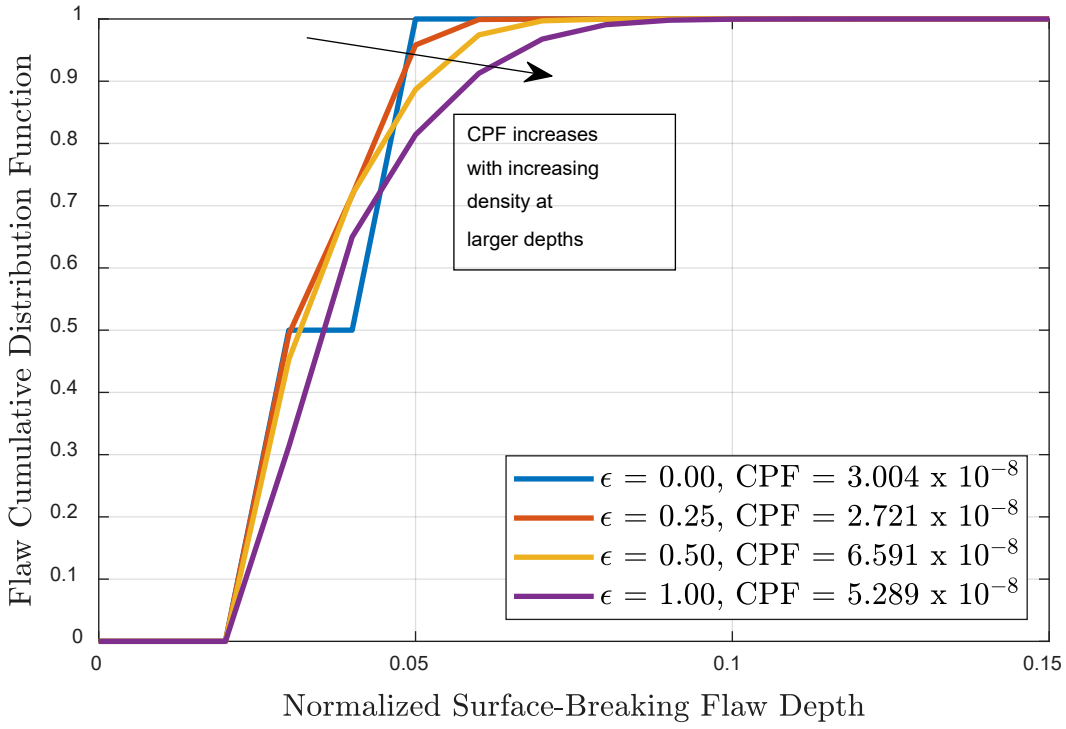

Figure 4-3: Empirical CDFs of flaw distributions for families of parameter uncertainty for mean CPF.

The mixed flaw case simulations (Scenarios 3 and 4) are not exactly what should be run as indicated by the flaw statistics. The results represent a necessary compromise to reflect the way FAVOR is coded. Effectively, once the sampling indicates the existence of an embedded flaw, the flaw files are scaled to include one surface-breaking flaw, Flaw A, and one embedded flaw, Flaw B. In reality, the uncertainty in flaw characteristics would mean that sometimes Flaw B is a surface flaw ('surface-breaking' case in Table 4-3 and Table 4-4; equivalent to saying that the likelihood of having an embedded flaw is zero), and other times it is an embedded flaw ('mixed' case in Table 4-3 and Table 4-4; equivalent to saying that the likelihood of having an embedded flaw is one). The results in Table 4-3 and Table 4-4 show that the existence of embedded flaws only slightly changes the probabilities of initiation and failure, so the assumption of all flaws as surface-breaking appears to be relatively accurate. Flaw statistics indicate that the likelihood of having an embedded flaw is between zero and one. Section 4.2.2 describes a study performed to account for this fact while being constrained within the coding structure of FAVOR.

4.2.2 Flaw Categorization Study

A subsequent study was formulated to consider how to best capture the true sampling statistics using the existing FAVOR input requirements. For example, under the sampling scheme described in Section 2.2, if parameter uncertainty, $\varepsilon = 1$, two surface-breaking flaws are obtained 75% of the time and one surface-breaking flaw and one embedded flaw are obtained 25% of time. Several approaches were explored to achieve the expected balance between sampled flaws:

- Flaw Scaling. Scale the flaw densities to get integer numbers of initial flaws as inputs and then rescale the predicted probabilities to represent the correct number of observed initial flaws.
- Modifying FAVOR Input Structure. Instead of duplicating the 1000 records in the flaw files, correctly distribute the flaw densities to reflect the statistical balance between realizations of surface-breaking and embedded flaws.

4.2.2.1 Flaw Scaling

In this approach, the number of observed flaws for each analysis has been scaled to observe the consequence on the prediction of CPI and CPF. Table 4-5 and Table 4-6 show selected results for CPI and CPF, respectively, with several surface-breaking and mixed flaw scenarios. Those scenarios consider the total number of initial flaws to be 2, 6, or 20; scale factors of 1, 3, and 10 respectively.

Table 4-5: Mean CPI for distributed flaw files with various parameter uncertainty

Parameter Uncertainty	Normal, Surface-Breaking			Normal, Mixed		
	2 Flaws	6 Flaws	20 Flaws	2 Flaws	6 Flaws	20 Flaws
0.00	9.369e-7	2.989e-6	1.054e-5	9.369e-7	2.992e-6	9.823e-6
0.05	9.369e-7	2.991e-6	1.066e-5	9.369e-7	2.302e-6	9.299e-6
0.25	8.015e-7	5.909e-6	2.013e-5	8.149e-7	4.681e-6	1.750e-5
1.00	1.744e-6	1.628e-5	4.448e-5	7.708e-6	7.708e-6	2.826e-5

Table 4-6: Mean CPF for distributed flaw files with various parameter uncertainty

Parameter Uncertainty	Normal, Surface-Breaking			Normal, Mixed		
	2 Flaws	6 Flaws	20 Flaws	2 Flaws	6 Flaws	20 Flaws
0.00	3.004e-8	9.596e-8	3.330e-7	3.004e-8	8.854e-8	2.994e-7
0.05	3.004e-8	9.612e-8	3.367e-7	3.004e-8	7.598e-8	3.003e-7
0.25	2.721e-8	1.917e-7	6.589e-7	2.651e-8	1.530e-7	5.406e-7
1.00	5.289e-8	6.329e-7	1.600e-6	3.297e-7	3.297e-7	8.775e-7

An observation from the above tables is that when all flaws are assumed to be surface-breaking, the predicted conditional probabilities for 6 and 20 flaws approximately scale proportionally with the probabilities predicted for 2 flaws. This suggests the reverse, namely, given a prediction for a large number of (non-interacting) flaws, the probabilities could be scaled to give a reasonable approximation for a smaller number of flaws. This may be useful in instances when cases are simulated where the statistics imply non-integer representations of different flaw-types. Due to the constraints imposed by the FAVOR flaw file structure, the theoretical distribution of flaw types could not be realized for small numbers of flaws for the cases shown in Table 4-5 and Table 4-6. Table 4-7 shows the flaws employed in analysis compared to the theoretical expectation.

Table 4-7: Fraction of Surface-Breaking Flaws in Mixed Analyses – Normal Sampling

Case	Parameter Uncertainty	Flaws			Theoretical Fraction
		2	6	20	
Default	0.00	1.0000	1.0000	1.0000	1.0000
3	0.05	0.5000	0.8333	0.9500	0.9987
6	0.25	0.5000	0.8333	0.8500	0.8536
8	1.00	0.5000	0.6667	0.7500	0.7545

Table 4-7 shows that the theoretical flaw distribution can be approximated better when more flaws are considered. The implication is that coupling of the detail given in the table with the previous observation of employing simple, post-prediction scaling suggests an ability to capture the underlying flaw statistics even if the uncertainty implies a non-integer value for flaw type. For example, if we are investigating a scenario with two observed flaws, with a parameter uncertainty given as $\varepsilon = 0.25$, running an analysis with 20 flaws (10 times the actual number) would allow us to approximately match the required ratio of surface-breaking and embedded flaws. Then scaling the CPI and CPF given in Table 4-5 and Table 4-6 would yield an approximate prediction for a total of two flaws with mixed character. In this case, Table 4-7 indicates that the flaw distribution should obtain 1.71 surface-breaking flaws and 0.29 embedded flaws. The predicted probabilities of initiation and failure are then, [CPI, CPF] = [1.750e-6, 5.406e-8]. Compare this to the case of all surface-breaking flaws, [CPI, CPF] = [2.013e-6, 6.589e-8], which indicates the expected conservatism for an assumption of surface-breaking flaws.

The following figures show expanded detail for the theoretical distribution of flaw type under both normal and uniform sampling over the modeled range of parameter uncertainty. Figure 4-4 shows the

theoretical fraction of surface-breaking flaws for the two sampling schemes. The observed inflection points are indicative of reaching thresholds of the physical constraints that are imposed on the sampling scheme.

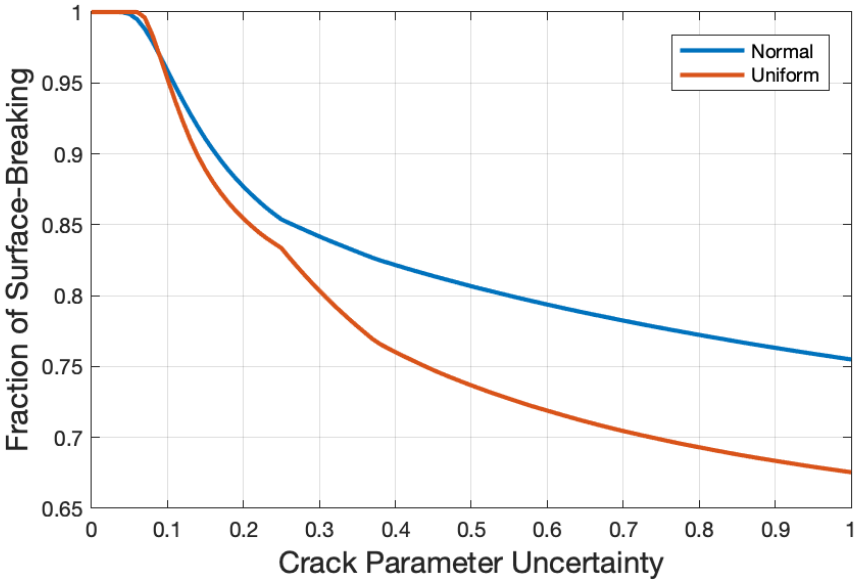

Figure 4-4**:** Theoretical fraction of surface-breaking flaws for $0 \leq \varepsilon \leq 1$**.**

Figure 4-5 is a continuous representation of the data that are contained in Table 4-7, shown for both uniform and normal sampling schemes. The theoretical curve for surface-breaking flaws should be used if the analysis is intended to preserve the sampling statistics used in the underlying model. The dashed lines show the manner in which the statistics are actually captured due to the constraints imposed by the FAVOR flaw input structure.

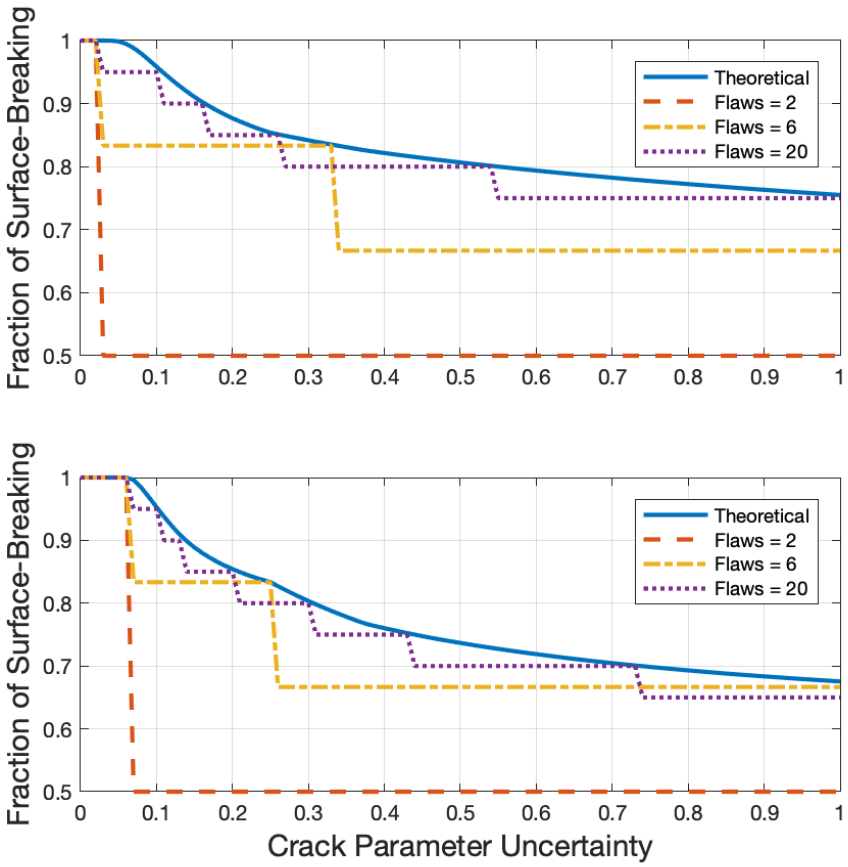

Figure 4-5: Convergence of FAVOR flaw statistics to theoretical statistics for normal (top) and uniform (bottom) sampling for $0 \leq \varepsilon \leq 1$.

4.2.2.2 Modifying FAVOR Input Structure

In the second approach, the flaw file input structure was modified so that the 1000 input records were not all identical, but rather were distributed in a manner consistent with the required flaw type. Again, if parameter uncertainty $\varepsilon = 1$, two surface-breaking flaws are obtained in 75% of the simulations and one surface-breaking flaw and one embedded flaw are obtained in 25% of the simulations. Therefore, the FAVOR input records were created such that approximately 75% of the records were appropriate for two surface-breaking flaws and the other 25% indicated one surface-breaking flaw and one embedded flaw. Table 4-8 shows the results of the study.

Table 4-8: Mean CPI/CPF for distributed flaw files with parameter uncertainty, $\varepsilon = 1$

Measure	Parameter Uncertainty	Normal, Mixed	Normal, Mixed, 2 Flaws N = 10000		Normal, Mixed, 2 Flaws N = 25000	
		2 flaws	Order A	Order B	Order A	Order B
CPI	1.00	7.708e-6	2.849e-6	3.654e-6	3.343e-6	3.648e-6
CPF		3.297e-7	9.884e-8	1.136e-7	1.414e-7	1.018e-7

The third column reports the CPI and CPF for ε = 1 under the assumption that Flaw A is always surface-breaking and Flaw B is always embedded. The flaw statistics were generated under the assumption that all of the sampled parameters were taken from a normal distribution. Again, this is not what the sampled statistics would indicate, but rather reflects a limitation in the manner in which FAVOR flaw files must be created. In reality, the sample statistics would indicate that Flaw B should be sampled as surface-breaking in 75.4% of the simulations and embedded in 24.6% of the simulations for ε = 1 (see Figure 4-4). Therefore, the fourth and fifth columns show the results for CPI and CPF when the flaw files are constructed such that: Order A - the first 754 records correspond to a surface-breaking Flaw B and the final 246 records correspond to an embedded Flaw B and Order B - the first 246 records correspond to an embedded Flaw B and the final 754 records correspond to a surface-breaking Flaw B. The order that the records appear in the flaw file will matter, due to how FAVOR samples, so the number of trials was increased to N = 25000 and the results are reported in the sixth and seventh columns. Consequently, it appears that the correct flaw distributions can be achieved using the existing FAVOR structure, using a sufficiently large number of trials.

4.2.2.3 Comparison of Approaches

A simple comparison of the two approaches can be made by interrogating Table 4-5, Table 4-6, and Table 4-8. For the case of normally sampled parameters with $\varepsilon = 1$, the flaw scaling approach predicts the probabilities of initiation and failure to be [CPI, CPF] = [2.826e-6, 8.775e-8], while modifying the FAVOR input structure predicts [CPI, CPF] ≈ [3.5e-6, 1.2e-7]. Although, not confirmatory, this comparison suggests the approaches may be reasonable means of capturing more complex representations of flaw statistics under an assumption of uncertainties in the measurement of flaw parameters.

5 STEP 5: DRAW CONCLUSIONS FROM ANALYSIS RESULTS

5.1 Step 5: Action 1 – Interpret analysis results

For the purposes of this analysis, the annual through-wall cracking (i.e. failure) frequency (TWCF) of 1×10^{-6} acceptance criteria was used. FAVOR was run using the inputs defined in Section 2 for the Plant 8 2007 normal cooldown transient at 48, 50 and 56 EFPY. Uncertainty was considered in the crack depth and length for both flaws, as well as in the fluence and embrittlement parameters.

After accounting for sampling uncertainty, a 95% confidence interval upper bound on the 99th percentile gives a conditional probability of failure (CPF) of 1.80e-7 at 48 EFPY (see Table 3-1.) As a reminder, the frequency of the transient considered is assumed to be 1 per year, so in this case, CPF=TWCF=1.80e-7 at 48 EFPY. Although the TWCF is lower than the acceptance criteria, the determination about whether acceptance criteria are met are typically not made based on just this calculation. A broad set of sensitivity studies was performed on the input parameters for the FAVOR analysis code. the results from those studies led to an investigation of a very specific set of uncertainties associated with the knowledge of the flaw parameters. Details of flaw parameter uncertainty is given in Section 4.2 and APPENDIX A.

5.2 Step 5: Action 2 – Iterate on analysis process to refine model results

Iteration on the FAVOR analysis led to a significant investigation into flaw parameter uncertainty. This analysis led to changes in the FAVOR flaw file input structure, refinements in input uncertainty distributions, explorations into different sampling schemes, convergence investigations, and the addition of sensitivity studies to identify conservative approaches for capturing flaw parameter uncertainty. These model refinements have been propagated into the results reported in Table 3-1.

6 REFERENCES

[1] L. Hund, J. Lewis, N. Martin, M. Starr, D. Brooks, A. Zhang, R. Dingreville, A. Eckert, J. Mullins, P. Raynaud, D. Rudland, D. Dijamco and S. Cumblidge, "NUREG/CR-7278: Guidance on Performing and Documenting Probabilistic Fracture Mechanics Analyses," U.S. Nuclear Regulatory Commission, Washington, DC, USA, 2021.

[2] P. Williams, T. Dickson, B. Bass and H. Klasky, "Fracture Analysis of Vessels - Oak Ridge FAVOR, v16.1, Computer Code: Theory and Implementation of Algorithms, Methods, and Correlations," Oak Ridge National Laboratory, Oak Ridge, TN, 2016.

[3] T. Dickson, P. Williams, B. Bass and H. Klasky, "Fracture Analysis of Vessels - Oak Ridge FAVOR, v16.1, Computer Code: User's Guide," Oak Ridge National Laboratory, Oak Ridge, TN, 2016.

[4] ASME, "American Society of Mechanical Engineers Boiler and Pressure Vessel Code - Sect. II, Part D: Properties," 1998.

[5] L. Stumpfrock and et.al, "Brittle Crack Initiation, Propagation and Arrest of Shallow Cracks in a Clad Vessel Under PTS Loading," NESC II Final Report, European Commission DG-JRC/IE, Petten, The Netherlands, 2003.

[6] E. Eason, G. Odette, R. Nanstad and T. Yamamoto, "A Physically Based Correlation of Irradiation-Induced Transition Temperature Shifts for RPV Steels," Oak Ridge National Laboratory, ORNL/TM-2006/530, 2006, 2006.

[7] A. Davison and D. Hinkley, Bootstrap Methods and Their Applications (Vol. 1), Cambridge University Press, 1997.

APPENDIX A FLAW STATISTICS

This section shows some graphical representations of the flaw distributions as a function of the parameter uncertainty, ε, and sampling approach.

A.1 All Flaws are Surface-Breaking

The following figures show the manner in which the crack parameters are distributed as a function of the parameter uncertainty under the assumption that all flaws are surface-breaking. Figure A-1 and Figure A-2 show how Flaw A depth is distributed for uniform and normal sampling schemes, respectively. Table A-1 provides discrete values of crack depth distributions for Flaw A at a selected set of crack parameter uncertainty values for uniform and normal sampling schemes. Figure A-3 and Figure A-4 show how Flaw B depth is distributed for uniform and normal sampling schemes, respectively. Table A-2 provides discrete values of crack depth distributions for Flaw B at a selected set of crack parameter uncertainty values for uniform and normal sampling schemes. Note that the actual sampling scheme allows for a continuous distribution of crack depths, but for the purposes of generating a FAVOR flaw file, the crack depths have been rounded to the nearest normalized vessel depth.

Inspection of Figure A-1 and Figure A-2 clearly demonstrate the difference in the sampling schemes. As expected, the normal sampling scheme manifests significantly lower uncertainty in flaw depth because of the shape of the distribution about the nominal flaw depth value. This observation is reinforced with the tighter distribution of flaw depths for a given parameter uncertainty value shown in Table A-1. This same observation holds for Flaw B as shown in Figure A-3, Figure A-4, and Table A-2.

Figure A-5 and Figure A-6 show how Flaw A aspect ratio is distributed for uniform and normal sampling schemes, respectively. Table A-3 provides discrete values of aspect ratio distributions for Flaw A at a selected set of crack parameter uncertainty values for uniform and normal sampling schemes. Figure A-7 and Figure A-8 show how Flaw B aspect ratio is distributed for uniform and normal sampling schemes, respectively. Table A-4 provides discrete values of crack depth distributions for Flaw B at a selected set of crack parameter uncertainty values for uniform and normal sampling schemes. Note that the actual sampling scheme allows for a continuous distribution of aspect ratios, but for the purposes of generating a FAVOR flaw file, the aspect ratios have been rounded up to the next largest aspect ratio bin designated for use by FAVOR (see Section 3.1).

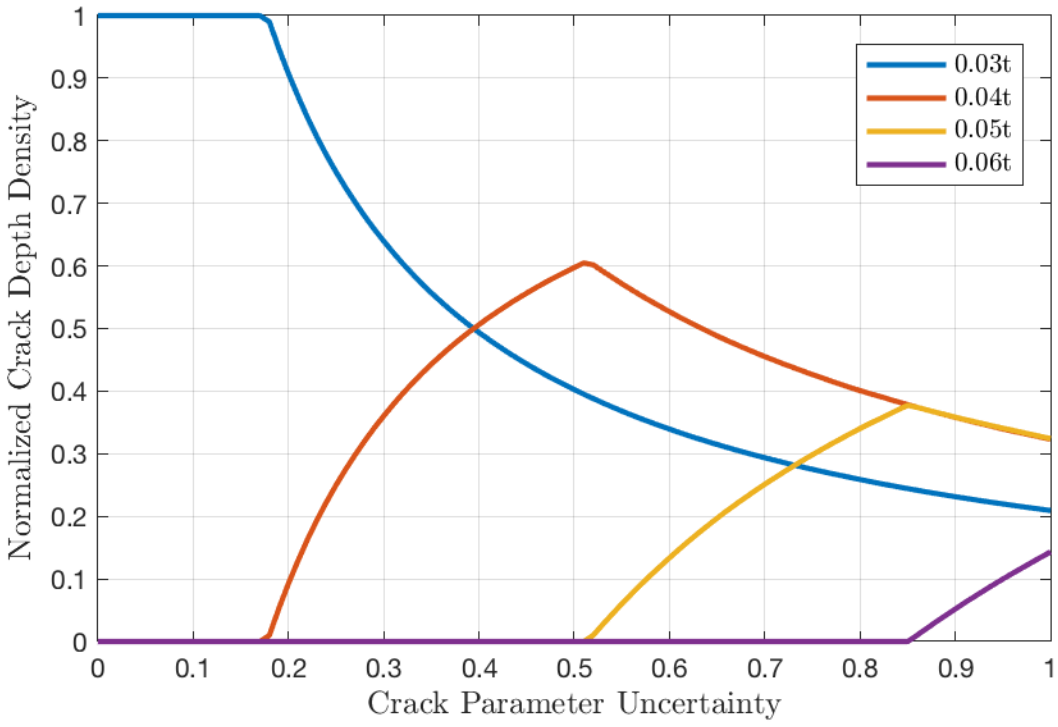

Figure A-1: Flaw A crack depth densities for uniformly sampled realizations.

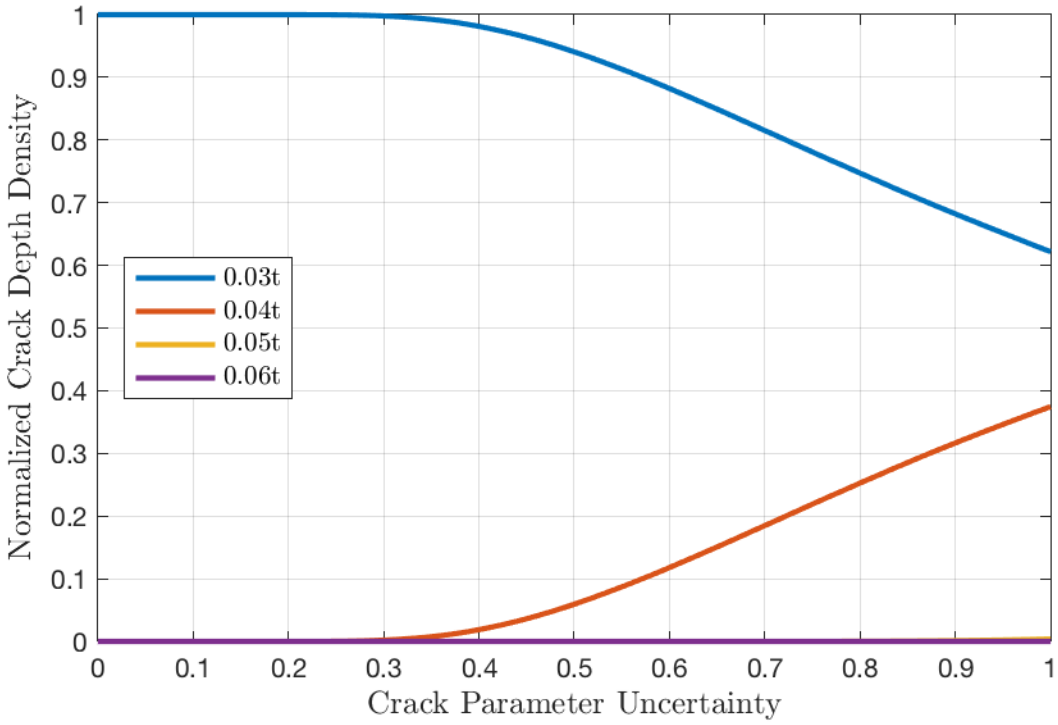

Figure A-2: Flaw A crack depth densities for normally sampled realizations.

Table A-1: Surface-breaking flaw depth density for selected parameter uncertainty, Flaw A

Sample Distribution	Crack Parameter Uncertainty ε	Normalized Crack Depth Density (Percentage of Flaws at a Given Normalized Vessel Depth)			
		0.03t	0.04t	0.05t	0.06t
Uniform	0	1.0000	0.0000	0.0000	0.0000
	0.5	0.4014	0.5986	0.0000	0.0000
	1	0.2077	0.3243	0.3241	0.1439
Normal	0	1.0000	0.0000	0.0000	0.0000
	0.5	0.9409	0.0591	0.0000	0.0000
	1	0.6213	0.3751	0.0036	0.0000

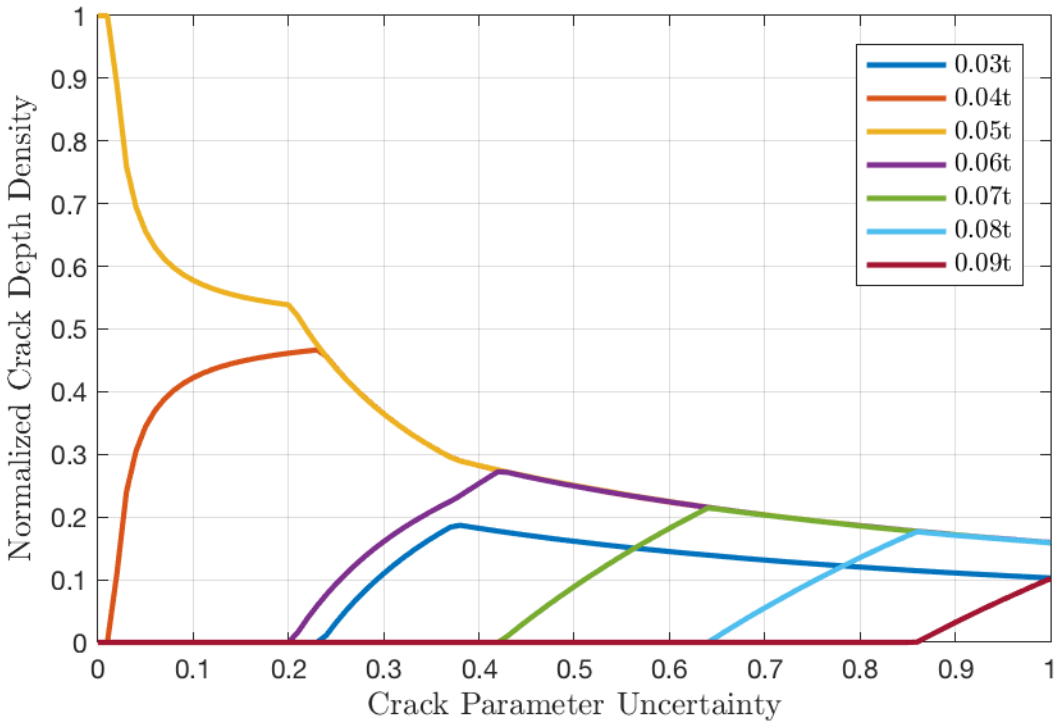

Figure A-3: Flaw B assumed surface-breaking, crack depth densities for uniformly sampled realizations.

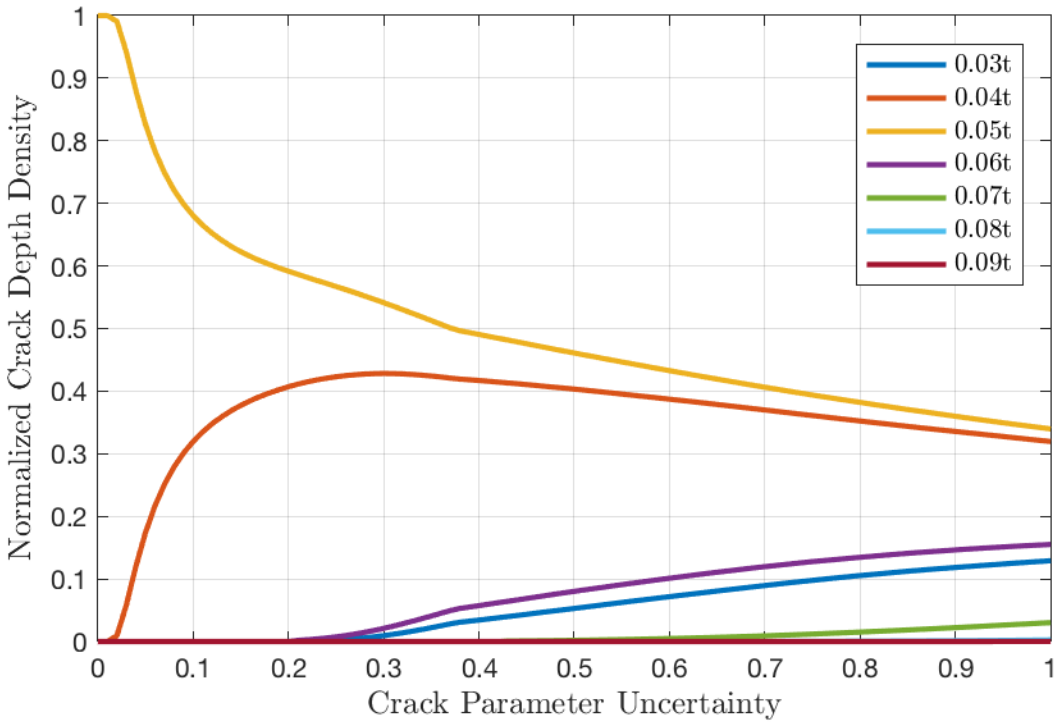

Figure A-4: Flaw B assumed surface-breaking, crack depth densities for normally sampled realizations.

Table A-2: Surface-breaking flaw depth density for selected parameter uncertainty, Flaw B

Sample Distribution	Crack Parameter Uncertainty ε	Normalized Crack Depth Density (Percentage of Flaws at a Given Normalized Vessel Depth)						
		0.03t	0.04t	0.05t	0.06t	0.07t	0.08t	0.09t
Uniform	0	0.0000	0.0000	1.0000	0.0000	0.0000	0.0000	0.0000
	0.5	0.1611	0.2496	0.2499	0.2502	0.0892	0.0000	0.0000
	1	0.1026	0.1590	0.1588	0.1586	0.1597	0.1590	0.1024
Normal	0	0.0000	0.0000	1.0000	0.0000	0.0000	0.0000	0.0000
	0.5	0.0532	0.4033	0.4606	0.0800	0.0019	0.0000	0.0000
	1	0.1292	0.3199	0.3396	0.1543	0.0303	0.0025	0.0001

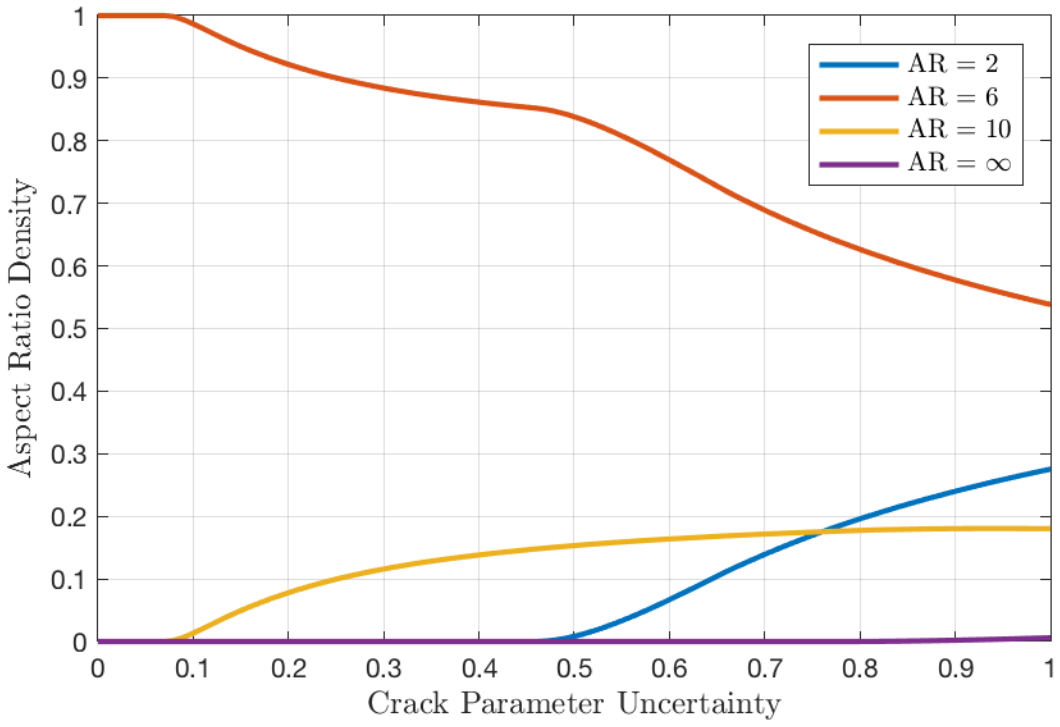

Figure A-5: Flaw A aspect ratio densities for uniformly sampled realizations.

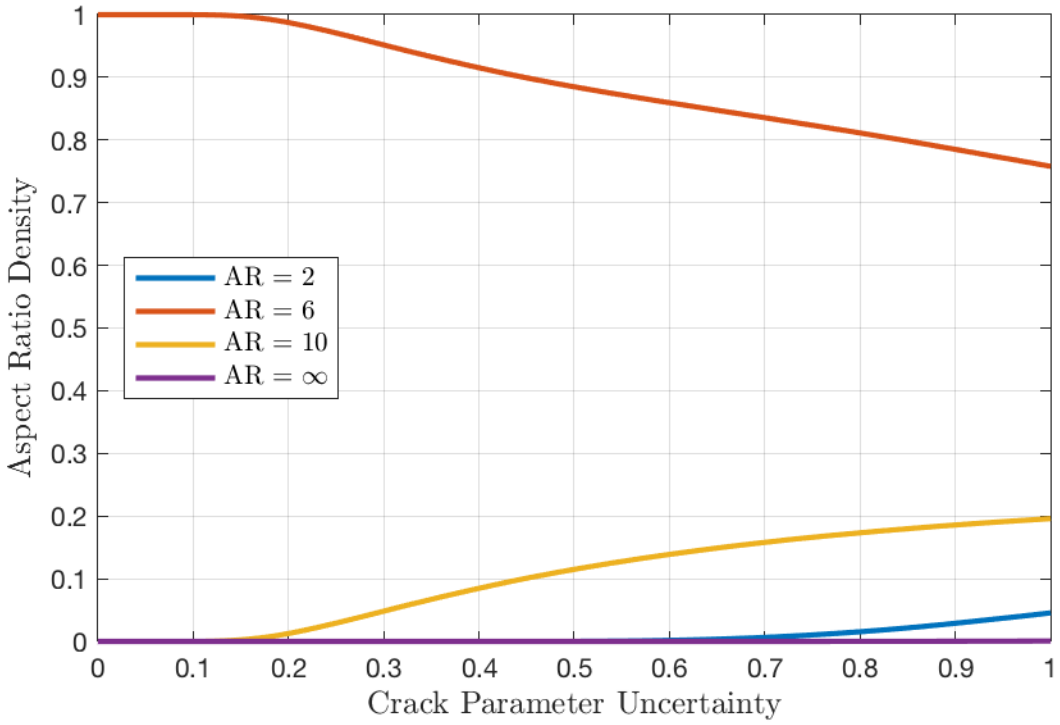

Figure A-6: Flaw A aspect ratio densities for normally sampled realizations.

Table A-3: Surface-breaking flaw aspect ratio density for selected parameter uncertainty, Flaw A

Sample Distribution	Crack Parameter Uncertainty ε	Normalized Aspect Ratio Density (Percentage of Flaws of a Given Aspect Ratio)			
		2	6	10	∞
Uniform	0	0.0000	1.0000	0.0000	0.0000
	0.5	0.0082	0.8393	0.1525	0.0000
	1	0.2753	0.5390	0.1797	0.0060
Normal	0	0.0000	1.0000	0.0000	0.0000
	0.5	0.0002	0.8853	0.1145	0.0000
	1	0.0458	0.7582	0.1954	0.0006

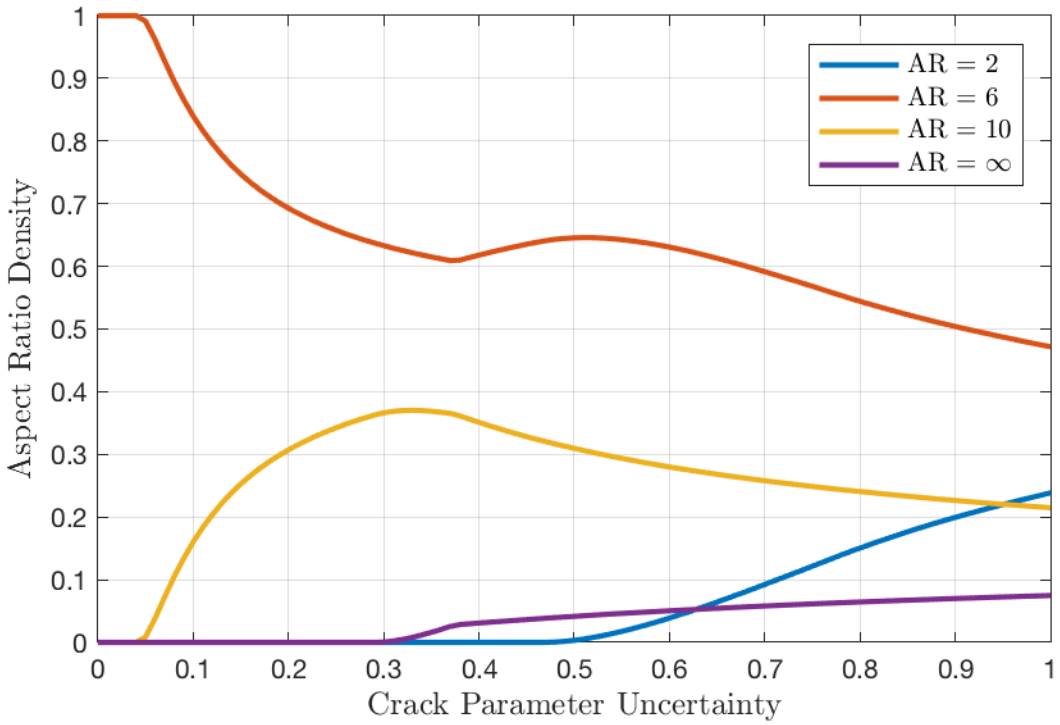

Figure A-7: Flaw B assumed surface-breaking, aspect ratio densities for uniformly sampled realizations.

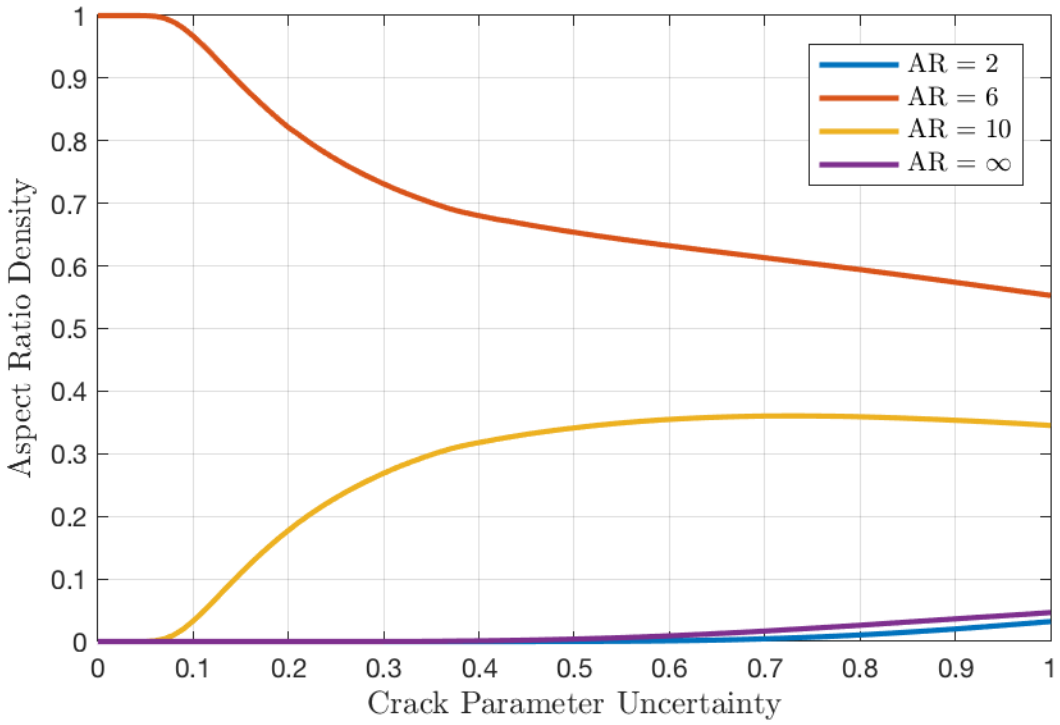

Figure A-8: Flaw B assumed surface-breaking, aspect ratio densities for normally sampled realizations.

Table A-4: Surface-breaking flaw aspect ratio density for selected parameter uncertainty, Flaw B

Sample Distribution	Crack Parameter Uncertainty ε	Normalized Aspect Ratio Density (Percentage of Flaws of a Given Aspect Ratio)			
		2	6	10	∞
Uniform	0	0.0000	1.0000	0.0000	0.0000
	0.5	0.0031	0.6461	0.3092	0.0416
	1	0.2385	0.4718	0.2152	0.0744
Normal	0	0.0000	1.0000	0.0000	0.0000
	0.5	0.0001	0.6532	0.3419	0.0038
	1	0.0320	0.5523	0.3453	0.0465

A.2 Flaws are of Mixed Character

The following figures show the manner in which the crack parameters are distributed as a function of the parameter uncertainty under the assumption that all the sampled Flaw A are surface-breaking and the sampled Flaw B are distributed between surface-breaking and weld-embedded (because all Flaw A are assumed to be surface-breaking, refer to Figure A-1, Figure A-2, Figure A-5, and Figure A-6, which are not reproduced here). Figure A-9 and Figure A-10 show the fraction of Flaw B that are embedded, as a function of the parameter uncertainty, for uniform and normal sampling schemes, respectively.

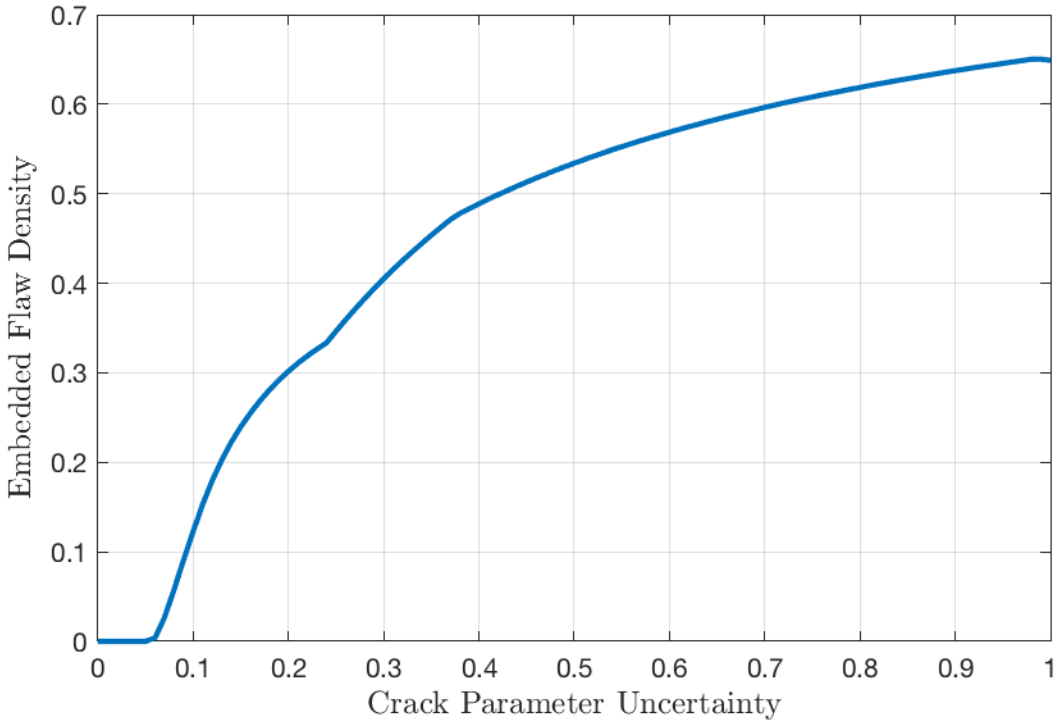

Figure A-9: Density of weld-embedded Flaw B for uniformly distributed sampling.

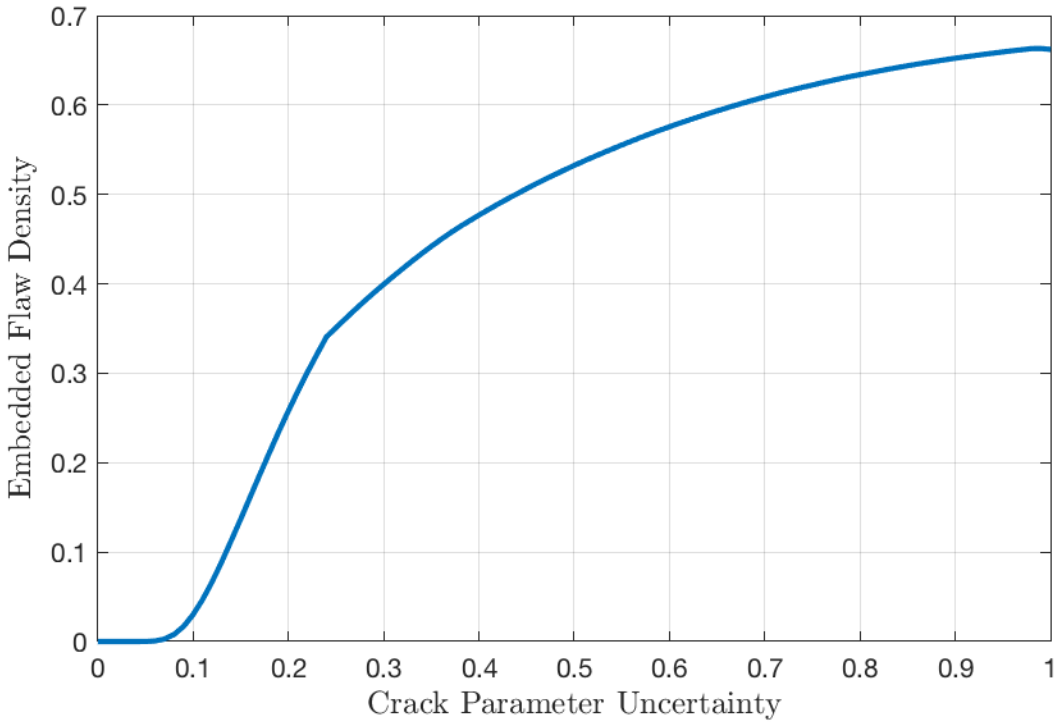

Figure A-10: Density of weld-embedded Flaw B for normally distributed sampling.

Figure A-11 and Figure A-12 show Flaw B depth distributions for uniform and normal sampling schemes, respectively. In both figures, the solid lines are families of surface-breaking flaws and the dashed lines are families of embedded flaws. Surface-breaking and embedded flaws of the same depth share the same color. Table A-5 provides discrete values of crack depth distributions for Flaw B, distributed across both flaw types, at a selected set of crack parameter uncertainty values for uniform and normal sampling schemes.

Figure A-13 and Figure A-14 show Flaw B aspect ratio distributions for uniform and normal sampling schemes, respectively. As with the crack depth plots, the solid lines are families of surface-breaking flaws and the dashed lines are families of embedded flaws. Note that in FAVOR, embedded flaws are binned in aspect ratios differently than surface-breaking flaws. However, all flaws were binned in the same way that surface-breaking flaws are categorized. .

Table A-6 provides discrete values of aspect ratio distributions for Flaw B, distributed across both flaw types, at a selected set of crack parameter uncertainty values for uniform and normal sampling schemes.

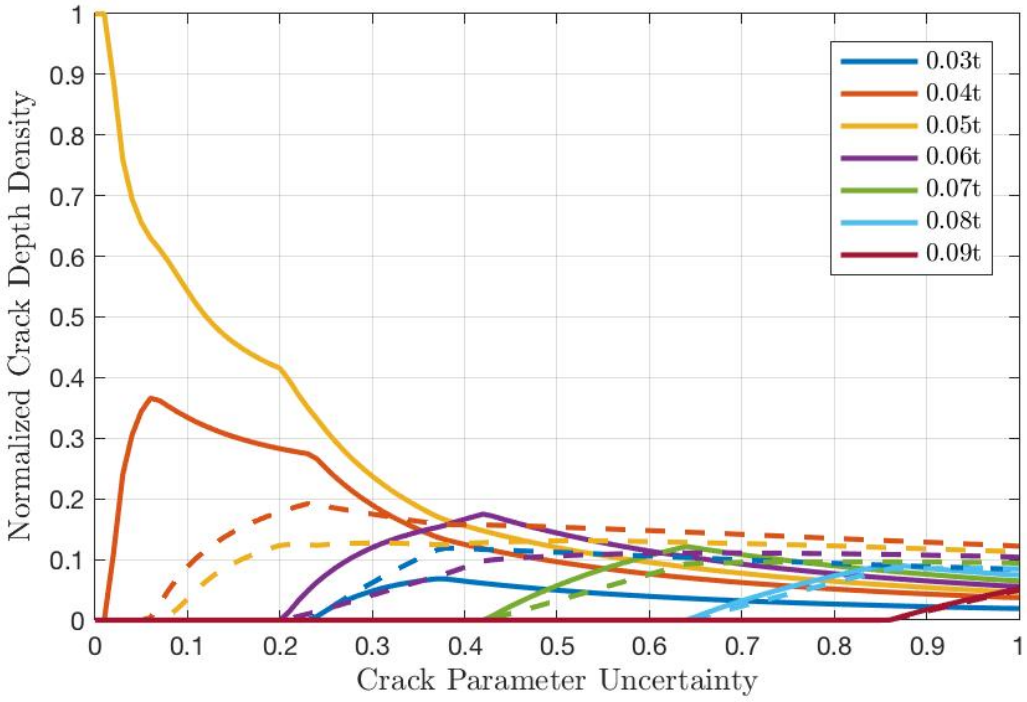

Figure A-11: Flaw B mixed character, surface-breaking flaws (solid) and embedded flaws (dashed), crack depth densities for uniformly sampled realizations.

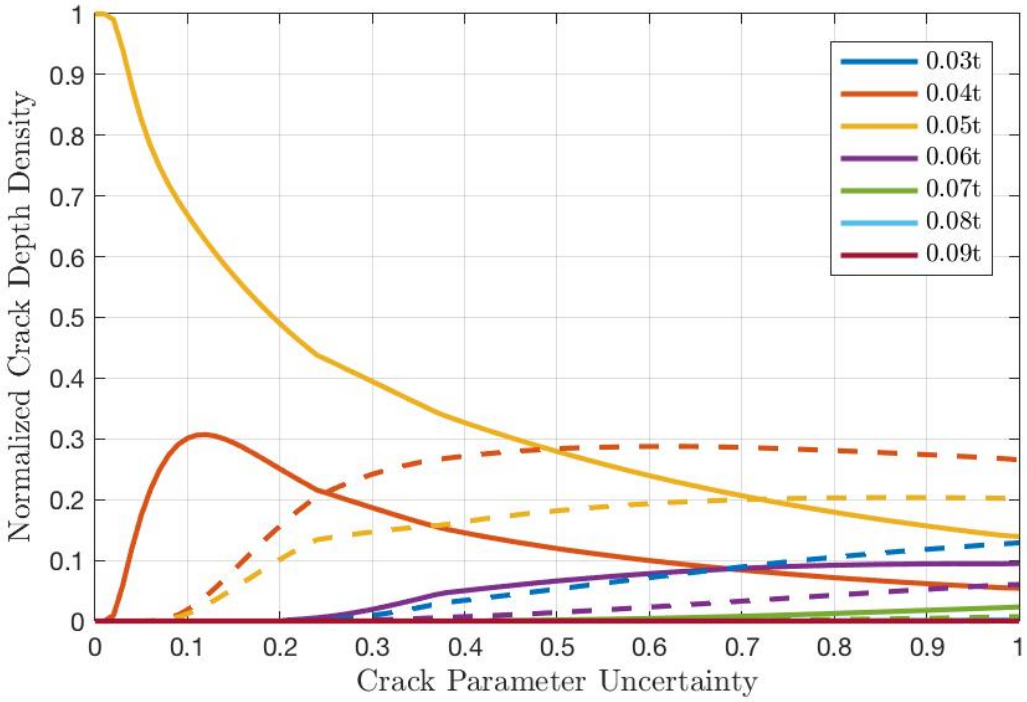

Figure A-12: Flaw B mixed character, surface-breaking flaws (solid) and embedded flaws (dashed), crack depth densities for normally sampled realizations.

Table A-5: Mixed flaw depth density for selected parameter uncertainty, Flaw B

Sample Distribution	ε	Flaw Type	Normalized Crack Depth Density (Percentage of Flaws at a Given Normalized Vessel Depth)						
			0.03t	0.04t	0.05t	0.06t	0.07t	0.08t	0.09t
Uniform	0	Surface	0.0000	0.0000	1.0000	0.0000	0.0000	0.0000	0.0000
		Embedded	0.0000	0.0000	0.0000	0.0000	0.0000	0.0000	0.0000
	0.5	Surface	0.0489	0.0956	0.1200	0.1437	0.0573	0.0000	0.0000
		Embedded	0.1114	0.1545	0.1303	0.1060	0.0322	0.0000	0.0000
	1	Surface	0.0191	0.0367	0.0466	0.0562	0.0651	0.0747	0.0529
		Embedded	0.0830	0.1219	0.1127	0.1030	0.0943	0.0841	0.0496
Normal	0	Surface	0.0000	0.0000	1.0000	0.0000	0.0000	0.0000	0.0000
		Embedded	0.0000	0.0000	0.0000	0.0000	0.0000	0.0000	0.0000
	0.5	Surface	0.0002	0.1199	0.2794	0.0655	0.0018	0.0000	0.0000
		Embedded	0.0530	0.2832	0.1825	0.0144	0.0001	0.0000	0.0000
	1	Surface	0.0001	0.0555	0.1423	0.0975	0.0237	0.0022	0.0001
		Embedded	0.1323	0.2709	0.2063	0.0615	0.0072	0.0003	0.0000

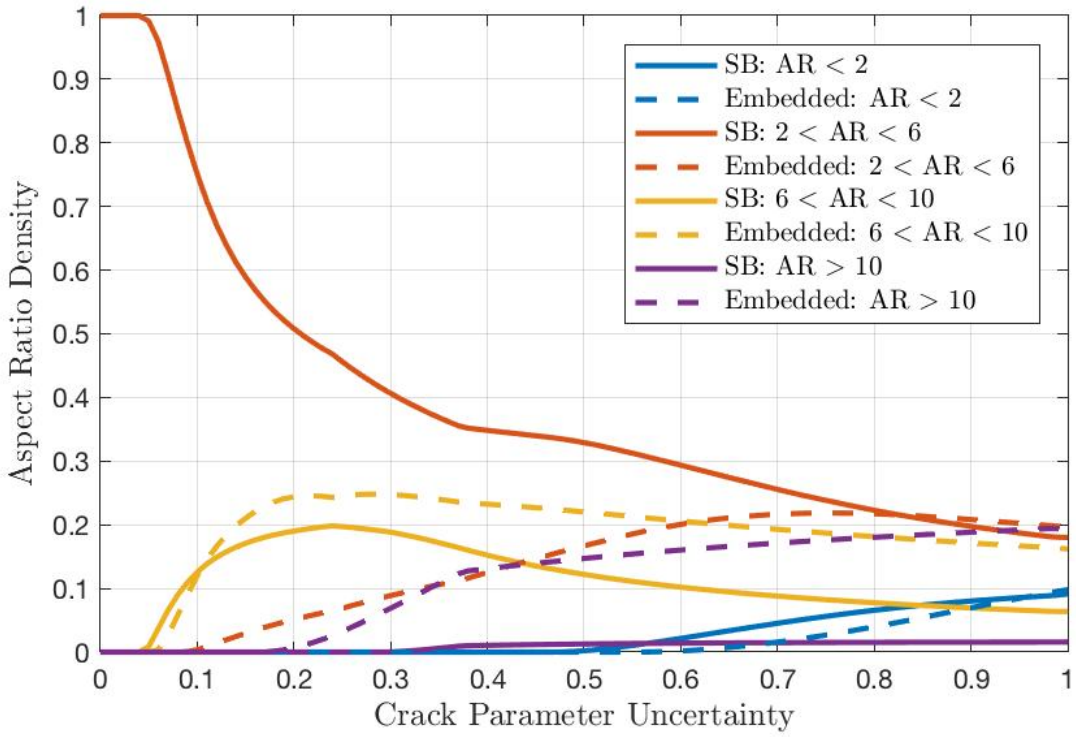

Figure A-13: Flaw B mixed character, surface-breaking flaws (solid) and embedded flaws (dashed), aspect ratio densities for uniformly sampled realizations.

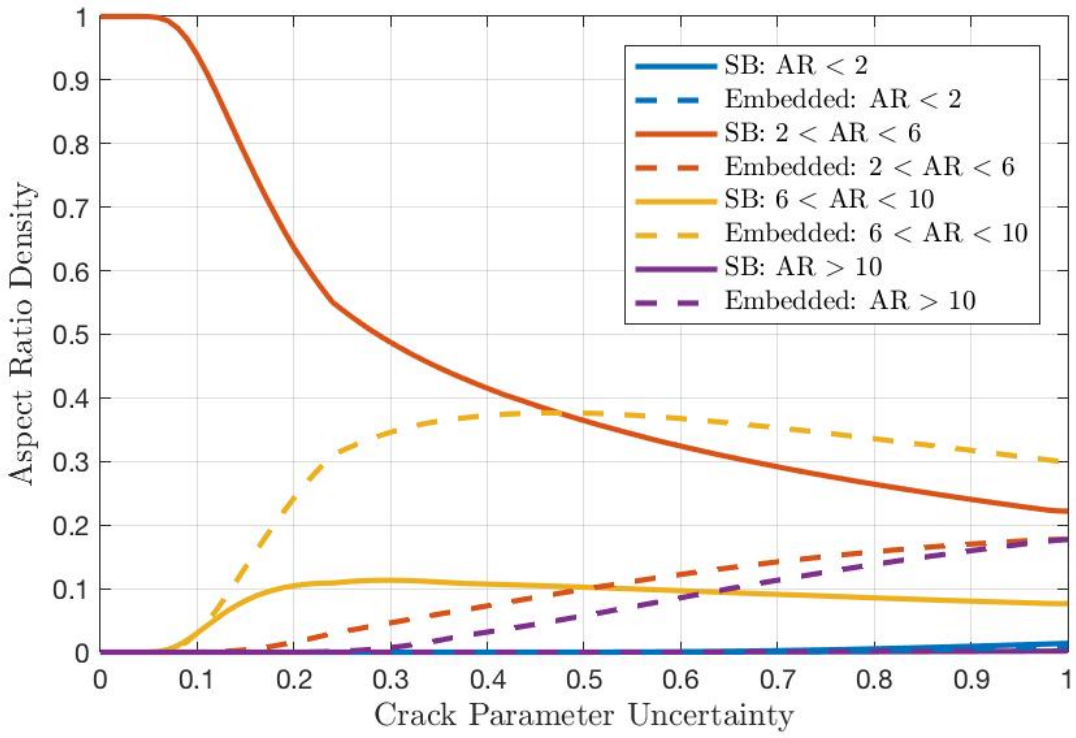

Figure A-14: Flaw B mixed character, surface-breaking flaws (solid) and embedded flaws (dashed), aspect ratio densities for normally sampled realizations.

Table A-6: Mixed flaw aspect ratio density for selected parameter uncertainty, Flaw B

Sample Distribution	ε	Flaw Type	Normalized Aspect Ratio Density (Percentage of Flaws of a Given Aspect Ratio)			
			2	6	10	∞
Uniform	0	Surface	0.0000	1.0000	0.0000	0.0000
		Embedded	0.0000	0.0000	0.0000	0.0000
	0.5	Surface	0.0021	0.3290	0.1218	0.0127
		Embedded	0.0000	0.1673	0.2206	0.1466
	1	Surface	0.0916	0.1801	0.0640	0.0156
		Embedded	0.0985	0.1961	0.1616	0.1925
Normal	0	Surface	0.0000	1.0000	0.0000	0.0000
		Embedded	0.0000	0.0000	0.0000	0.0000
	0.5	Surface	0.0001	0.3643	0.1023	0.0000
		Embedded	0.0000	0.0990	0.3762	0.0581
	1	Surface	0.0143	0.2271	0.0780	0.0020
		Embedded	0.0100	0.1811	0.3048	0.1824

A.3 Uncertainty for SMiRT Analysis

The uncertainty chosen for SMiRT analysis was $\varepsilon = 0.25$. This was arbitrary, but loosely based on the observation that some flaw detection techniques have limitations to detection. One observation suggested there may only be a 50% likelihood of detecting a flaw 0.04 inches in depth and 95% likelihood of detecting a flaw 0.08 inches in depth. Consequently, it is not unrealistic to assume that a similar order of magnitude of error in depth characterization could be applied to the flaws reported in the SMiRT problem statement. Based on the previous sensitivity studies, in general, using a normal distribution when sampling the crack parameters yields more conservative predictions for CPI and CPF.

The figures below show scatter plots of the raw sampled crack parameters under consideration for all the combinations of flaw type and sampling scheme. Figure A-15 and Figure A-16 show Flaw A and B distributions for uniform and normal sampling schemes, respectively, if both are assumed to be surface-breaking. Figure A-17 and Figure A-18 show Flaw A and B distributions for uniform and normal sampling schemes, respectively, if Flaw A is surface-breaking and Flaw B has mixed character.

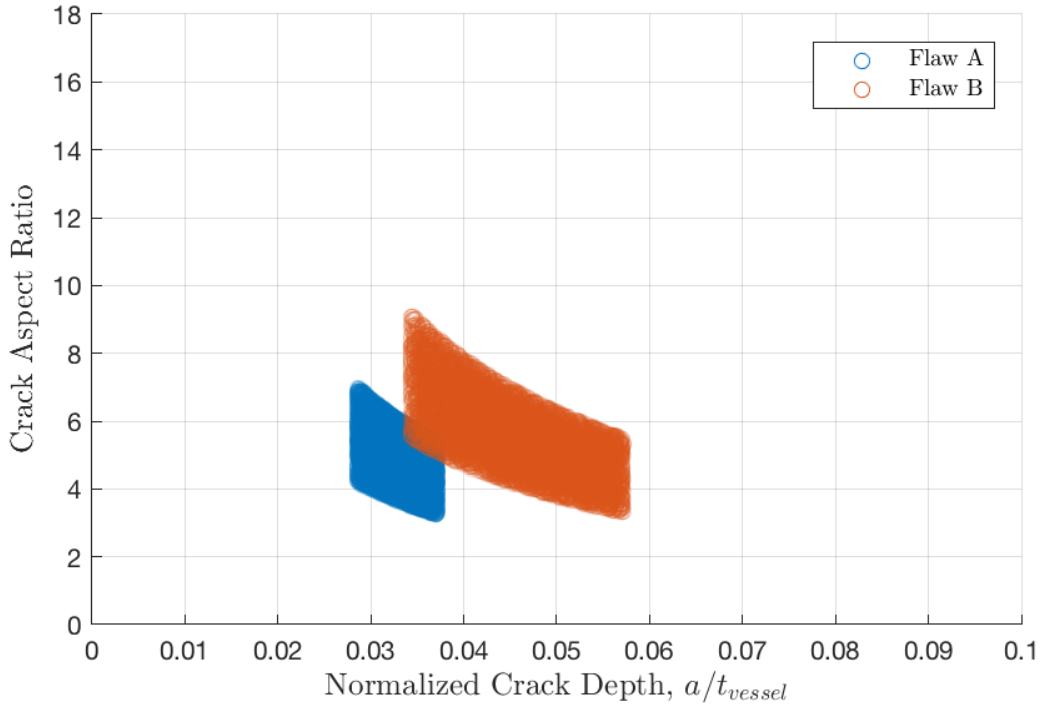

Figure A-15: Sampled parameter space for uniformly sampled surface-breaking realizations, ε = 0.25.

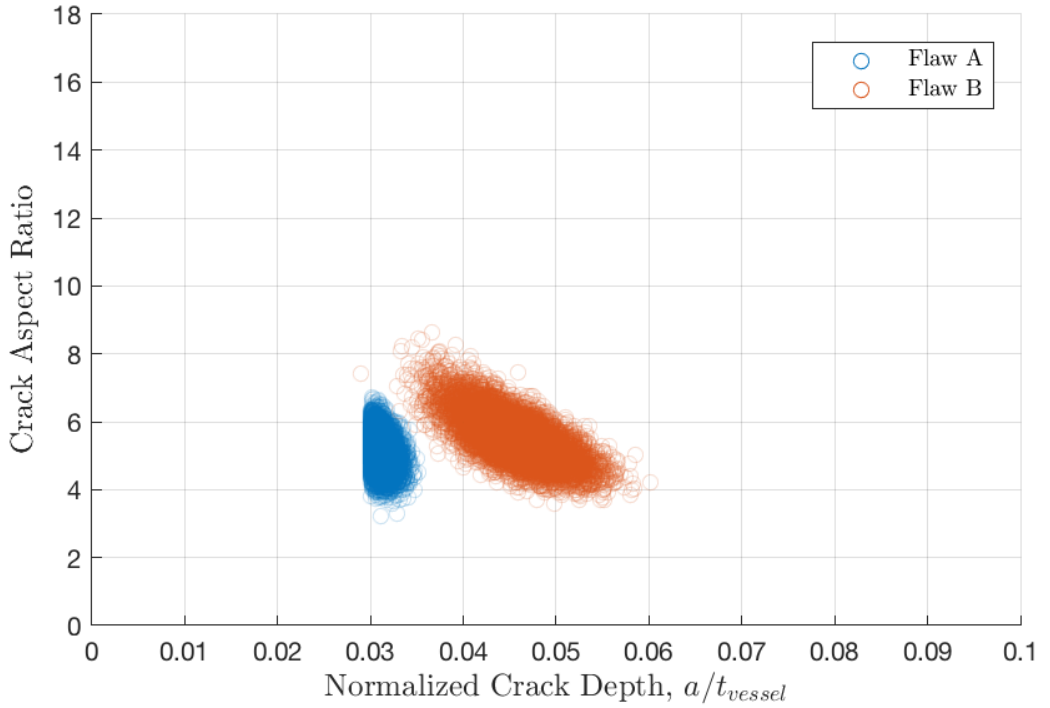

Figure A-16: Sampled parameter space for normally sampled surface-breaking realizations, ε = 0.25.

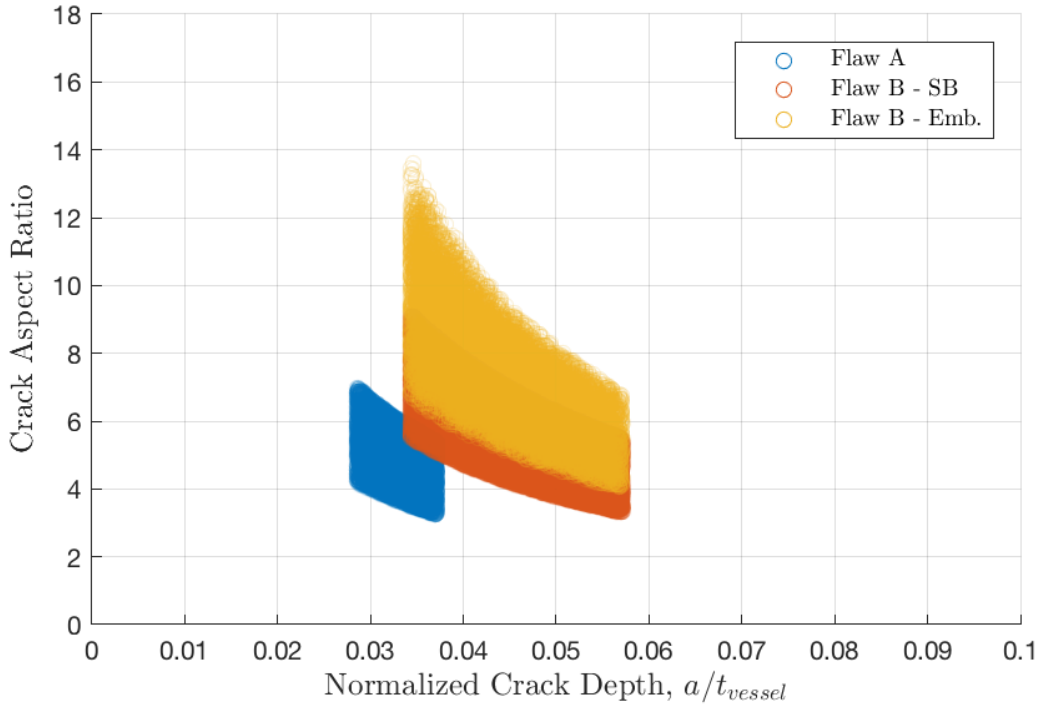

Figure A-17: Sampled parameter space for uniformly sampled mixed character realizations, ε = 0.25.

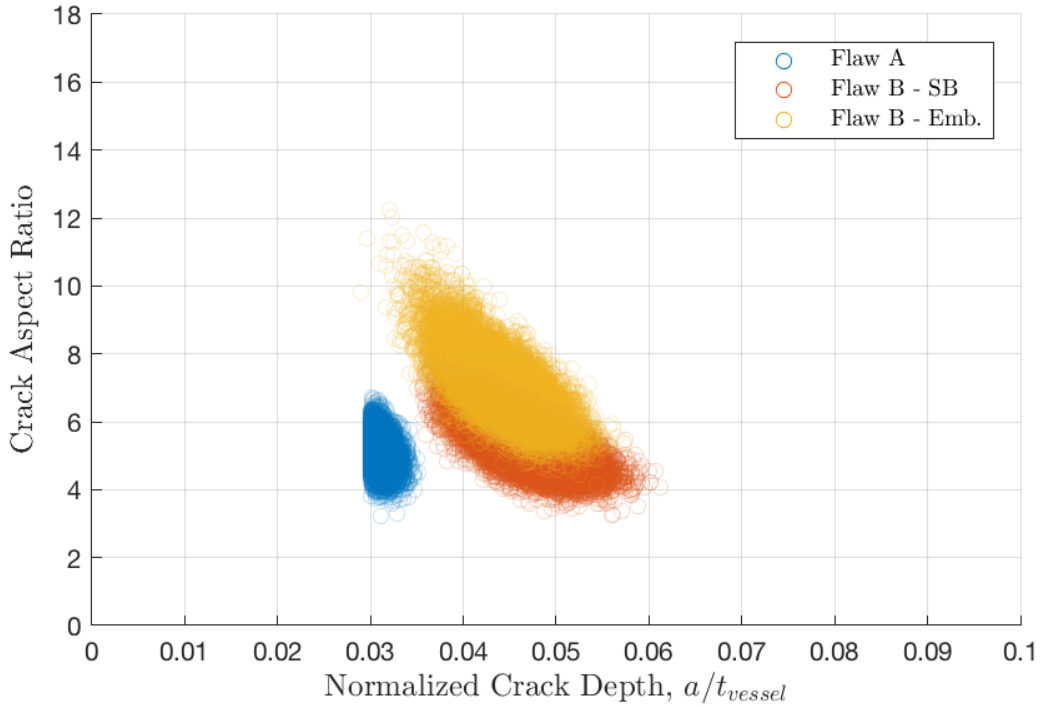

Figure A-18: Sampled parameter space for normally sampled mixed character realizations, ε = 0.25.

APPENDIX B ADDITIONAL PROBLEM STATEMENT DETAILS

This appendix outlines some temperature-dependent information necessary for the FAVOR Application Study that was not included in Section 2.

B.1 Deterministic FAVLoad Tables

Table 2-1 describes the deterministic inputs for FAVLoad; however, some of those inputs are temperature dependent. These thermal and mechanical properties of the base and clad, which are derived from information in the ASME Boiler and Pressure Vessel Code [4], are described in this section. The thermal conductivity and specific heat of the base and clad are shown in Table B-1. Young's Moduli and coefficients of thermal expansion are detailed in Table B-2 and Table B-3, respectively.

Table B-1: Deterministic thermal properties in FAVLoad input

	BASE Thermal Properties		CLAD Thermal Properties	
Temperature [°F]	**Conductivity [BTU/(hr ft)]**	**Specific Heat [BTU/(lbm°F)]**	**Conductivity [BTU/(hr ft°F)]**	**Specific Heat [BTU/(lbm°F)]**
70	24.8	0.1052	8.1	0.1158
100	25.0	0.1072	8.4	0.1185
150	25.1	0.1101	8.6	0.1196
200	25.2	0.1135	8.8	0.1208
250	25.2	0.1166	9.1	0.1232
300	25.1	0.1194	9.4	0.1256
350	25.0	0.1223	9.6	0.1258
400	25.1	0.1267	9.9	0.1281
450	24.6	0.1277	10.1	0.1291
500	24.3	0.1304	10.4	0.1305
550	24.0	0.1326	10.6	0.1306
600	23.7	0.1350	10.9	0.1327
650	23.4	0.1375	11.1	0.1335
700	23.0	0.1404	11.4	0.1348
750	22.6	0.1435	11.6	0.1356
800	22.2	0.1474	11.9	0.1367

Table B-2: Young's Moduli used in deterministic FAVLoad input

BASE Property		CLAD Property	
Temperature [°F]	**Young's Modulus [Mpsi]**	**Temperature [°F]**	**Young's Modulus [Mpsi]**
70	29.2	68	22.05
200	28.5	302	20.16
300	28.0	482	18.42
400	27.4		
500	27.0		
600	26.4		
700	25.3		
800	23.9		

Table B-3: Coefficients of thermal expansion used in FAVLoad deterministic inputs

	BASE Property	CLAD Property
Temperature [°F]	**Coefficient of Thermal Expansion [1/°F]**	**Coefficient of Thermal Expansion [1/°F]**
100	7.06	8.55
150	7.16	8.67
200	7.25	8.79
250	7.34	8.90
300	7.43	9.00
350	7.50	9.10
400	7.58	9.19
450	7.63	9.28
500	7.70	9.37
550	7.77	9.45
600	7.83	9.53
650	7.90	9.61
700	7.94	9.69
750	8.00	9.76
800	8.05	9.82

B.2 FAVPFM Embrittlement Map Data

To estimate irradiated values for RTNDT, FAVOR requires detailed neutron fluence and chemistry data. These parameters are outlined in this section. For an example of embrittlement map input to FAVOR, see Figure 4-1. Table B-4 details the fluence for each point in the reactor operating history and Table B-5 provides the nominal chemical compositions, which are constant for all analyses.

Table B-4: Deterministic fluence data in FAVPFM input

Region	48 EFPY Fluence [10^{19} n/cm^2]	50 EFPY Fluence [10^{19} n/cm^2]	56.5 EFPY Fluence [10^{19} n/cm^2]	72 EFPY Fluence [10^{19} n/cm^2]
1	2.1241	2.1816	2.3683	2.8135
2	2.6524	2.7393	3.0219	3.6958
3	2.6524	2.7393	3.0219	3.6958
4	2.6802	2.7690	3.0575	3.7456
5	2.1408	2.1991	2.3889	2.8412
6	2.6802	2.7690	3.0575	3.7456
7	3.4041	3.5104	3.8559	4.6797
8	3.4010	3.5071	3.8522	4.6750
9	3.4010	3.5071	3.8522	4.6750
10	3.4010	3.5071	3.8522	4.6750
11	3.4346	3.5430	3.8950	4.7346
12	3.4346	3.5430	3.8950	4.7346
13	3.4346	3.5430	3.8950	4.7346

Table B-5: Deterministic chemistry data in FAVPFM input

Region	Copper [wt%]	Nickel [wt%]	Phosphorus [wt%]	Manganese [wt%]
1	0.231	1.01	0.019	1.315
2	0.231	1.01	0.019	1.315
3	0.231	1.01	0.019	1.315
4	0.231	1.01	0.019	1.315
5	0.231	1.01	0.019	1.315
6	0.231	1.01	0.019	1.315
7	0.203	1.018	0.013	1.147
8	0.190	0.48	0.016	1.24
9	0.190	0.50	0.015	1.24
10	0.120	0.55	0.010	1.27
11	0.240	0.51	0.009	1.24
12	0.240	0.50	0.010	1.35
13	0.240	0.50	0.011	1.29